*fibers*

MDPI

*Review*

# Converging Electrospinning and 3D-Printing Technologies: From Innovative Design for Tissue Engineering to Global Patent Trends and Technology Transfer

**Karen J. Juarez-Navarro [1,2], Vincenzo Guarino [3,*] and Marco A. Alvarez-Perez [2,*]**

[1] Posgrado en Ciencias Biológicas, Facultad de Ciencias, Universidad Nacional Autónoma de México, Av. Ciudad Universitaria 3000, Mexico City C.P. 04510, Mexico; k.juarezn118@gmail.com
[2] Laboratorio de Bioingeniería de Tejidos, División de Estudios de Posgrado e Investigación, Facultad de Odontología, UNAM, Circuito Exterior s/n Cd. Universitaria, Mexico City C.P. 04510, Mexico
[3] Institute of Polymers, Composite and Biomaterials, National Research Council of Italy, Mostra d'Oltremare, Pad 20, V.le J.F.Kennedy 54, 80125 Naples, Italy
* Correspondence: vincenzo.guarino@cnr.it (V.G.); marcoalv@unam.mx (M.A.A.-P.)

## Highlights

**What are the main findings?**

- We propose a scoping review to demonstrate the innovative aspects of a new technological approach based on the integration of 3D-printing and electrospinning manufacturing techniques.

**What is the implication of the main finding?**

- The accurate description of relevant examples focused on 3D printing/electrospinning integration allowed us to remark on the distinctive aspects of different approaches, suggesting a prospective use in scientific research on tissue engineering and translational medicine.

**Abstract:** Electrospinning is a technique that enables the production of nano- and microfibrillar patterns that mimic the native extracellular matrix. However, these nanofibrous structures often lack mechanical properties suitable for reproducing the behavior of structurally complex tissues. Therefore, achieving more accurate and precise geometric structures be-comes a key challenge. In this context, additive manufacturing techniques such as 3D printing may allow for the development of tailored structures with highly controlled ar-chitecture and improved mechanical strength. However, in contrast with electrospinning, these techniques are commonly considered "low-resolution" techniques, unable to ma-nipulate structural details at the submicrometric scale. Hence, this review aims to intro-duce and discuss recent technological approaches based on combining these technologies for scaffold development in tissue engineering, detailing some distinct integration strate-gies correlating the outcomes to the benefits and drawbacks. Finally, a comprehensive analysis of the current state of the art in the registered intellectual property related to these integrated approaches will be proposed, assessing their distribution by geographic region and analyzing the main trends over time and future fallouts.

**Keywords:** nanofibers; additive manufacturing; multi-scale porosity; scaffolds; tissue engineering; electrospinning

check for updates

Academic Editor: Martin J. D. Clift

Received: 18 April 2025
Revised: 21 May 2025
Accepted: 10 June 2025
Published: 19 June 2025

**Citation:** Juarez-Navarro, K.J.; Guarino, V.; Alvarez-Perez, M.A. Converging Electrospinning and 3D-Printing Technologies: From Innovative Design for Tissue Engineering to Global Patent Trends and Technology Transfer. *Fibers* **2025**, *13*, 83. https://doi.org/10.3390/fib13060083

**Copyright:** © 2025 by the authors. Licensee MDPI, Basel, Switzerland. This article is an open access article distributed under the terms and conditions of the Creative Commons Attribution (CC BY) license (https://creativecommons.org/licenses/by/4.0/).

## 1. Introduction

Tissue engineering (TE) is a multidisciplinary field that aims to repair, regenerate, or create damaged tissues and organs. Tissue engineering is also based on the interaction of three key components: scaffold, cells, and biological factors essential for the complete and functional development of complex tissues [1]. In this context, a scaffold is a three-dimensional structure designed to support and guide cell growth in a controlled environment. Scaffolds used in TE must have important characteristics such as biocompatibility, biodegradability, promoting cell adhesion and proliferation, adequate mechanical strength, structural precision, and good transport properties to support successful targeted tissue regeneration [2]. Basically, "a good scaffold" should mimic or replicate the conditions of the extracellular matrix of the target tissue. Nowadays, there are different techniques and materials to manufacture scaffolds in TE, and it is important to consider that the scaffold manufacturing technique determines the material's structure, porosity, and mechanical properties [3]. These factors directly affect cellular interaction, vascularization, and the functionality of the generated tissue [4,5]. Recently, the electrospinning technique has gained popularity as it allows the obtention of nano- (<1000 nm) and microfibrillar (1 μm–100 μm) patterns that make it possible to obtain surfaces that resemble the extracellular matrix (ECM), offering a high surface area, tunable porosity, and the capacity to incorporate bioactive molecules [6–8]. However, electrospun scaffolds lack the mechanical stability and geometric control required for complex tissue applications.

On the other hand, using 3D printing for TE scaffold fabrication leads to precise control over scaffold architecture. It enables the design of customizable and tailored shapes and precise geometrical patterns but struggles to achieve the nanoscale resolution needed to mimic native tissue at the cellular level [9]. Therefore, the combination of electrospinning and 3D printing overcomes the individual limitations of these technologies [10]. This hybrid approach produces scaffolds that integrate nanoscale features for cellular interaction with macroscale designs that provide structural integrity. Such scaffolds have shown promise in tissue-specific applications, including bone regeneration, skin wound healing, and nerve repair.

This review explores the integration of electrospinning and 3D printing for scaffold fabrication and their TE application, highlighting and discussing their advantages, various fabrication methods, assessments, results, and specific applications in TE. Additionally, we performed extensive research on patent registries and analyzed the global patent landscape and emerging innovations, detailing the various fabrication methods of combination, applications, and results that position this hybrid strategy as a pivotal tool to advance regenerative medicine. To our knowledge, this is the first review to comprehensively examine the patent landscape associated with integrating electrospinning and 3D printing for tissue engineering.

## 2. Fundamentals of Electrospinning

Electrospinning is a process in which thin fibers are produced by applying a strong electric field to a polymer solution or melt, overcoming the liquid's surface tension, which causes the polymer to be drawn out into fine fibers, which are then deposited on a collector [11]. The main components of an electrospinning process are the spinneret or ejector system, the collector, and the high-power voltage source (Figure 1). The ejector system or spinneret often consists of a syringe through which a polymer solution is extruded at a constant rate controlled by a pump. Both the spinneret and the collector are connected to a high-voltage source. Usually, the spinneret is supplied with a positive or negative charge while the collector gains an opposite polarity; this creates an electromagnetic field, and the repulsive forces between the charges disrupt the superficial tension of the pendant solution

drop and deform its spherical shape into a cone (Taylor cone); at the tip of this cone, and due to the electrostatic forces, a polymer solution jet is emitted and rapidly elongated before depositing into the collector. During this elongation process, the solvent is evaporated and the final result is thin polymer fibers with reduced diameters [12,13].

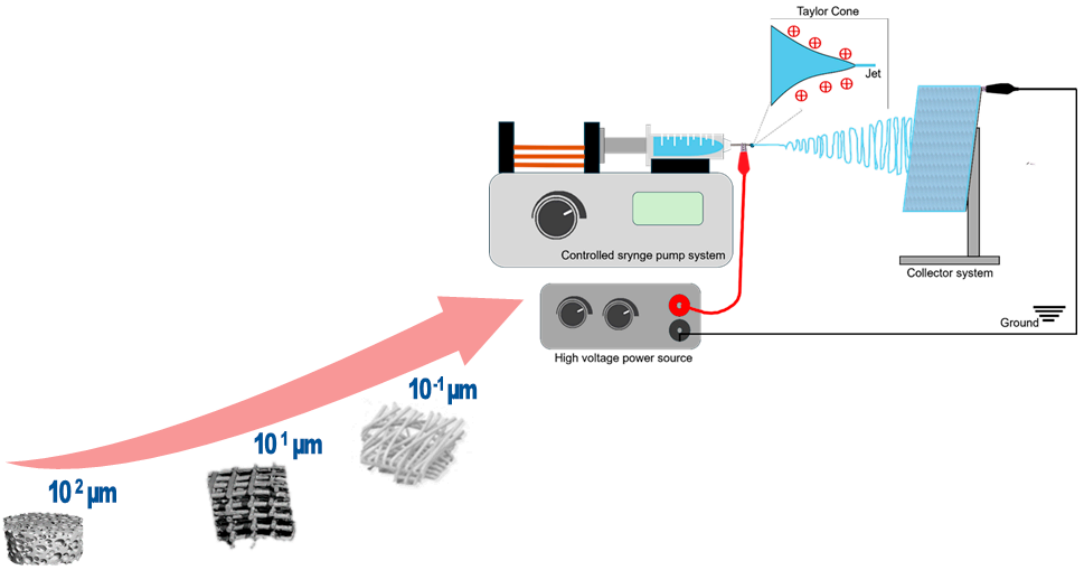



**Figure 1.** From micro- to nanoscale: schematic illustration of the electrospinning process and setup.

### *2.1. Solution and Polymer Parameters*

Polymer parameters such as molecular weight and concentration directly affect the solution's viscosity; hence, the fiber diameters are obtained through electrospinning. Previous works have established a relation between polymer molecular weight and fiber results. It has been reported that lower molecular weights prevent fiber formation and result in just beads, while higher molecular weights allow uniform fibers, as described in Figure 2. For example, Alharbi et al. (2023) tested different polycaprolactone (PCL) molecular weights and concentrations and assessed the final fiber diameter. Their results showed that fibers are more uniform at higher molecular weights than low molecular weights and concentrations [14].

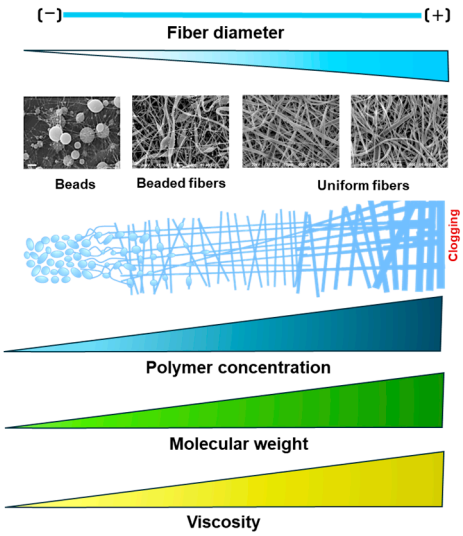



**Figure 2.** Effect of solution parameters on fiber morphology during the electrospinning process.

Furthermore, a low polymer concentration or molecular weight leads to less viscosity, which decreases fiber formation and produces beads instead of fibers (electrospraying).

On the contrary, a higher polymer molecular weight or concentration increases viscosity, promoting uniform fiber formation. However, if the viscosity exceeds a critical threshold, it obstructs the solution's flow through the needle tip, potentially leading to clogging [15–17].

Additionally, solvent choice is crucial as it affects viscosity and influences the solution's dielectric constant, modulating its charge distribution and directly impacting the electrospinning process [18]. For instance, a higher dielectric constant in the solvent has been shown to significantly reduce the diameter of electrospun fibers [19]. It has been reported that solutions with higher conductivity lead to bead-free fibers [20]. The solvent selection also affects the surface morphology and crystallinity of the electrospun fibers. Thus, choosing the right solvent system is vital, considering that a "good solvent" should efficiently dissolve the polymer, have moderate volatility to facilitate solvent evaporation during electrospinning, and ensure the solution has the proper viscosity and surface tension for stable jet formation and fiber stretching [21].

### *2.2. Process Parameters*

Various parameters, including voltage, flow rate, and tip-to-collector distance, influence the final fiber diameter in the electrospinning process. As previously mentioned, the applied voltage at a critical value during electrospinning induces the polymer droplet to deform and stretch into a Taylor cone, breaking its superficial tension and producing fibers; this is why voltage is considered an essential parameter in determining the quality of electrospun fibers. The critical voltage value varies depending on the polymer system and should be optimized based on the desired fibrous morphology. In electrospinning, the applied voltage typically ranges from 10 to 25 kV, the current is in the nano (nA) to milliampere (mA) range (1 nA to 2 mA), with a resulting electrical power ranging approximately between 0.01 and 25 watts, depending, of course, on the applied voltage, flow rate, and solution properties [22,23]. Theoretically, one could infer that the fiber diameter decreases at higher voltages as the electrical field between the spinneret and the collector becomes more vigorous, causing greater stretching forces on the polymer jet. Comparative studies of electrospinning parameters have reported that greater voltage values lead to finer fibers; for instance, when comparing 10 to 15 kV and 12–18 kV, it was found that the highest voltage conditions (15 and 18 kV, respectively) reduced the fiber diameter [24,25]. However, this is not a universal rule; there are reports on how higher voltages produce wider fibers than lower voltages under the same process conditions, and not only can higher voltage levels induce fiber thickening but they can also promote bead and non-uniform fiber population production. For example, when comparing different voltage conditions, the highest voltage increased the fiber diameter and bead formation (20 kV) [26]. Also, Liu et al. (2019) reported a fiber diameter decrease from 6 to 20 kV, then an increase again at higher voltages (>20 kV) due to the reduction in field strength per jet leading to thicker fibers and broader diameter distribution [27]. Therefore, the voltage must be optimized carefully, as the data show varying results, and fiber formation depends on the voltage and solution parameters that were previously discussed.

Another crucial process parameter in electrospinning that influences fiber morphology is the distance between the needle and the collector, as it directly affects the polymer jet's flight time and the solvent evaporation rate. Recent findings have shown that increasing the electrospinning distance reduces fiber diameter and improves fiber uniformity [24,28,29]. A greater distance allows for better solvent evaporation and elongation of the jet, resulting in thinner and more homogeneous fibers. Conversely, if the distance is excessive, it may negatively impact fiber quality by producing more beads, as noted in various studies that indicate that bead formation can occur at both inadequate and excessive distances [30].

Additionally, the flow rate plays a crucial role in determining the characteristics of electrospun fibers. For instance, Hasanzadeh et al. found that lower flow rates resulted in thinner fibers and more uniformity within the fiber population. Similarly, Ranjbar reported that decreased flow rates produce thinner fibers, while an increase in flow rate yields thicker fibers. Inconsistency, Herrero-Herrero reported that although the diameter of the fibers tends to increase with higher flow rates, this effect is relatively weak. Furthermore, faster flow rates can cause bead formation and thicker fibers due to limited drying time before reaching the collector, which reduces the stretching forces [29,31,32]. In addition to the flow rate, needle gauge, and diameter, the needle also plays a critical role in determining the shear rate and, consequently, the fiber morphology. Considering a constant volumetric flow rate with variations in needle gauge, a smaller needle diameter increases the shear rate, which in turn reduces the fiber diameter. For example, He et al., (2019) investigated the effect of different needle diameters on fiber size and concluded that smaller needles lead to higher shear rates and finer fibers, whereas larger needle diameters favor the production of thicker fibers [33].

### *2.3. Environmental Parameters*

Environmental factors, including temperature and humidity, significantly impact the properties of electrospun fibers. Recent studies have highlighted the critical role of humidity in the electrospinning process, which affects fiber morphology, structural integrity, and mechanical properties. Low humidity leads to the formation of beads, whereas higher humidity levels produce bead-free, porous fibers [34]. Also, increasing humidity reduces fiber diameter significantly, implying tighter fiber spinning and a transition to more ductile yet structurally weaker fibers as humidity levels rise [35]. Studies indicate that increased humidity smooths and reduces the porosity of fibers from hydrophobic polymers. At the same time, it significantly delays solvent evaporation for hydrophilic polymers, allowing extended fiber stretching and resulting in finer fibers. However, excessive humidity can delay solvent evaporation in hydrophilic polymers, leading to beaded fibers and a loss of control over fiber morphology, resulting in lower fiber quality, poor mechanical properties, and irregular structures [36]. Therefore, it is essential to keep a humidity balance to ensure fiber quality, process production, and repeatability.

Additionally, temperature affects the drying rate of the fiber during electrospinning, influencing fiber morphology and quality. Studies have shown that high temperatures facilitate faster solvent evaporation, producing smoother and more uniform fibers. It has been reported that phase separation is noticeable at a controlled temperature of 20 °C, resulting in rough fiber surfaces, particularly when combined with higher humidity levels. However, as the temperature increases to 40 °C, these irregularities diminish at lower humidity conditions (30% RH), suggesting smoother fiber outcomes [37]. This highlights the sensitive balance required in managing environmental conditions during electrospinning to ensure the production of high-quality fibers tailored for specific applications.

## 3. Biomedical Applications for Electrospun Nanofibers

Electrospun fibers have emerged as promising materials in the biomedical field. They offer a unique combination of a high surface area, tunable porosity, and customizable properties, supporting various applications. As this review primarily focuses on biomedical applications, particularly in TE, the discussion will delve into the robust potential of electrospun fibers to enhance scaffold design and support complex tissue regeneration processes.

### *3.1. Electrospinning for Tissue Engineering*

Tissue engineering is an interdisciplinary field that integrates principles from biology, medicine, and engineering to create biological substitutes that repair, maintain, or improve tissue function [38]. This field addresses the limitations of traditional treatments like organ transplantation, such as donor shortages and immune rejection [39]. TE strategies often employ scaffolds designed to mimic the extracellular matrix, facilitating cell attachment, proliferation, and differentiation, essential for regenerating tissue structure and function [40].

Electrospinning has become a valuable tool in TE for fabricating nanofibrous scaffolds that resemble the natural ECM architecture [41]. These electrospun scaffolds offer a high surface-to-volume ratio and tunable porosity, supporting cell migration and nutrient exchange qualities, making them ideal for diverse TE applications [42]. This section will summarize how electrospinning contributes to developing effective scaffolds for tissue regeneration.

#### 3.1.1. Bone

Several reports on electrospun scaffolds with tailored properties for bone TE show significant progress in this field, demonstrating bioactivity, cell compatibility, and mechanical integrity advancements. For instance, Meng et al. (2024) reported the development of a 3D sponge-like scaffold composed of electrospun poly-l-lactic acid (PLLA) and PCL fibers integrated with bioactive glass (BG) particles. Their design resulted in a scaffold with enhanced bioactivity, improved mechanical properties, and cell compatibility. The interconnected pores (~335.3 μm) facilitated significant osteoblast proliferation (281.6% by day 10), highlighting the scaffold's potential to mimic ECM environments. The addition of BG enhanced hydrophilicity (contact angle reduced to 79.7°) and mechanical strength (compressive modulus improved to 6.1 ± 0.4 kPa) [43].

Similarly, Kalidas and Sumathi (2024) fabricated electrospun gelatin/polyvinyl alcohol/silk fibroin (GT/PVA/SF) scaffolds reinforced with copper-substituted hydroxyapatite (Cu-HAP). Their CGPS 16 scaffold (60 wt% Cu-HAP) exhibited exceptional mechanical strength (tensile strength of 96.13 MPa, Young's modulus of 995.78 MPa) and biological activity. With a porosity of 99%, the scaffold facilitated cell viability and proliferation and supported osteogenic differentiation, as evidenced by increased alkaline phosphatase (ALP) activity. Also, they assessed the scaffold antimicrobial activity with significant inhibition zones against *E. coli*, *S. aureus*, and *C. albicans*. This study emphasizes the scaffold's potential to promote bone healing while preventing microbial infections [44].

Additionally, PCL/Starch/CaO scaffolds have shown biomineralization and hydroxyapatite (HA) formation after 28 days of in vitro use, indicating the scaffold's capacity to support mineral deposition; in vivo testing also demonstrated a favorable tissue response, with the scaffold showing controlled resorption, advantageous for applications where gradual degradation aligns with tissue regeneration [45]. Also, poly-lactic acid (PLA) fibers infused with bioactive glass and magnesium oxide (MgO) nanoparticles have been shown to promote osteogenic differentiation through enhanced ALP expression and HA formation on the fiber surfaces simulated natural bone mineralization, while MgO's antimicrobial properties reduced *Staphylococcus aureus* (*S. aureus*) viability, positioning the PLA composite as a multifunctional scaffold capable of supporting bone regeneration and minimizing infection risk [46].

Expanding on scaffold applications in bone engineering, there are reports of electrospun scaffolds for controlled drug release to target prosthetic infections; for example, Boncu et al. (2020) evaluated linezolid-loaded poly(lactic-co-glycolic acid) (PLGA) and PLGA/PCL electrospun fiber mats for controlled drug release and reported that both fiber

types effectively inhibited methicillin-resistant *S. aureus* growth in vitro, with sustained antibiotic release. These scaffolds also exhibited in vivo biocompatibility, as demonstrated by the absence of significant inflammation, suggesting their utility in infection control within prosthetic devices [47]. Another innovative approach and application of electrospun scaffolds in TE is reported by Danfang Sun et al. (2024), where electrospun PCL-based scaffolds incorporating up-conversion nanoparticles (UCNPs) and MgO simultaneously supported bone regeneration and enabled non-invasive monitoring of scaffold degradation. The P1U1M scaffold, optimized with 1% MgO, showed enhanced biocompatibility, balanced degradation, and improved ALP activity (1.82-times higher than PCL by day 4). Notably, in vivo studies confirmed significant bone regeneration around skull defects in rats and the ability to track scaffold degradation via fluorescence imaging over 28 days [48]. This combination of functionality and monitoring capability underscores the versatility of electrospinning in creating multifunctional scaffolds.

#### 3.1.2. Skin

Several recent studies have contributed significant advancements in electrospun nano- and microfibrous scaffolds for skin TE applications, emphasizing their biocompatibility, antibacterial properties, and functional wound and skin healing enhancement. To illustrate, Anjum et al. (2023) demonstrated that polyvinylpyrrolidone and polyvinyl alcohol (PVP/PVA) nanofiber scaffolds provided a non-toxic, biocompatible environment for fibroblasts and red blood cells, with promising subcutaneous biocompatibility in rats due to their slow degradation and minimal inflammatory response [49]. Focused on burn healing, Shadman-Manesh et al. (2023) utilized PCL and polyethylene glycol (PEG), supplemented with egg yolk oil, which yielded antibacterial effects, improved cell viability, and superior healing in full-thickness burns, enhancing collagen synthesis and re-epithelialization in comparison to the control groups [50]. Likewise, Lizarazo-Fonseca et al. (2023) contributed a collagen-enhanced PCL scaffold with Wharton's jelly mesenchymal stromal cells, achieving structured tissue organization and improved skin morphology in a porcine model [51]. Other researchers recently proposed using asymmetric membranes—namely, two fibrous layers with different compositions/architecture—to mimic the heterogeneous composition of skin tissue, i.e., epidermis and dermis. In this case, a sequential strategy was investigated to collect layer-by-layer electrospun fibers: In particular, the top layer consisted of cross-linked PVA nanofibers to replicate the epidermis's chemical stability and wettability features. Otherwise, the bottom layer was fabricated by integrating PVA with wool-keratin to improve the cell interface [52].

Electrospun scaffolds are, therefore, tailored according to the tissue engineering goal. Research groups have explored their functionalization by incorporating drugs, antioxidants, or *Lactobacillus* to enhance their antibacterial and skin-restorative effects, such as the addition of *Lactobacillus plantarum (L. plantarum)* within polyurethane (PU)-based scaffolds, which provides antibacterial effects against common wound pathogens and enhanced cellular proliferation in vitro and improved wound closure and increased angiogenesis in vivo [53]. Similarly, Du et al. (2023) enhanced electrospun silk fibroin/gelatin (SF/GT) scaffolds with propolis, resulting in increased antibacterial activity against *Escherichia coli (E. coli)* and *S. aureus*, promoting cell migration and wound healing; this was further tested in an in vivo mouse skin defect model demonstrating hemocompatibility and accelerated healing [54]. Petrova et al. (2024) added cerium oxide nanoparticles (CeONPs) to chitosan/polyethylene oxide (CS/PEO) electrospun nanofibers, resulting in enhanced oxidative protection and cell attachment, while in a rat model, the scaffold displayed stable tissue integration and reduced inflammation [55].

Furthermore, recent findings have shown the potential of nanofiber-based scaffolds in promoting wound healing, particularly for diabetic wounds. These scaffolds aim to enhance re-epithelialization and improve overall healing outcomes by integrating therapeutic agents or synthetic fiber matrices, offering promising alternatives to traditional treatments. For example, Ali et al. (2023) developed a PLA-based multilayer scaffold carrying therapeutic agents (phenytoin, sildenafil citrate, and simvastatin) for sustained release, resulting in significant re-epithelialization and organized cell layers without scar tissue by the end of 21 days in a diabetic wound rat model [56]. Note well that this approach for diabetic wound healing has recently been tested in a clinical trial as a diabetic foot ulcer treatment (DFU); during this randomized controlled trial, the effectiveness of a synthetic electrospun fiber matrix (SEFM) was evaluated and compared against the standard treatment. Among patients with DFUs, 74% of wounds treated with SEFM achieved 100% re-epithelialization in 12 weeks, reducing healing time, versus 33% in the standard care group [57].

#### 3.1.3. Cardiac and Vascular Tissues

Recent research on vascular and cardiac TE scaffolds has focused on developing biomaterials with specific mechanical, biocompatibility, and regenerative properties to enhance cardiovascular repair, interestingly exploring the efficacy of electrospun scaffolds through in vitro and in vivo models. Recently, a GT-PCL electrospun scaffold engineered for small-diameter artery reconstruction was created, showing high structural integrity and endothelial viability in vitro and a favorable hemostatic performance with minimal inflammation in a swine pulmonary artery model [58]. Similarly, Xiao et al. (2024) developed a core/shell PLGA/PCL structure through electrospinning, resulting in grafts with excellent mechanical stability, low inflammatory response, and effective re-endothelialization in a rat abdominal aorta model over 12 months, supporting its long-term applicability for vascular grafting [59].

For myocardial applications, Wei et al. (2023) developed a cardiac patch incorporating an electrospun PCL–silk fibroin matrix and carbon nanotubes (CNTs), which promoted cardiomyogenic differentiation and displayed enhanced conductivity. In a myocardial infarction model, this patch significantly improved angiogenesis, reduced inflammation, and facilitated cardiomyocyte regeneration, suggesting a strong potential for cardiac function recovery [60]. Similarly, Liu et al. (2024) designed a polyurethane electrospun nanofiber (DINN) incorporating salvianic acid A for sustained anti-inflammatory and angiogenic effects. In the myocardial infarction rat model and arterial repair, DINN promoted myocardial function recovery and the rapid re-endothelialization of arterial grafts, illustrating the advantage of the integration of bioactive components in modulating cellular responses and reducing oxidative stress [61]. Additionally, Handley and Callanan (2023) incorporated ascorbic acid into PCL electrospun nanofibers, which diminished reactive oxygen species and demonstrated high cytocompatibility with endothelial cells, supporting its use in oxidative stress reduction for cardiac engineering [62]. Furthermore, Liu et al. (2023) reported the combination of PCL with human placental ECM to create an immune-modulatory scaffold that enhanced macrophage polarization and endothelial cell proliferation, showing significant improvements in endothelialization and smooth muscle regeneration in a rat artery model [63].

Researchers have explored synthetic and hybrid materials to enhance blood compatibility in cardiovascular applications. For instance, Chernonosova et al. (2024) developed an electrospun Carbothane™ scaffold blended with GT, which showed improved cell adhesion and endothelial compatibility in vitro. This scaffold demonstrated superior graft patency and biological compatibility in a rat model compared to commonly used expanded polytetrafluoroethylene vascular grafts [64]. These findings highlight the benefits of using hybrid

and bioactive scaffolds, each designed to address specific challenges in cardiovascular applications, including mechanical durability, biocompatibility, anti-inflammatory effects, and support for tissue regeneration.

#### 3.1.4. Cartilage, Ligament, Muscle, and Tendons

Recent studies on electrospun scaffolds for cartilage, ligament, and tendon TE show innovative approaches designed to enhance tissue repair by incorporating bioactive components into electrospun mats, modifying their structural alignment, or using them as advanced delivery systems. For instance, Xie et al. (2024) developed a PLLA electrospun scaffold combined with barium titanate to provide piezoelectric properties to the scaffold, and they added Fibroblast Growth Factor-18 (FGF-18) for its delivery. This synergy between controlled piezoelectrical stimulation and growth factor release supported cartilage repair. In vitro, the scaffold enhanced chondrocyte proliferation and ECM production, while in a rabbit cartilage defect model, it promoted ECM remodeling and effective cartilage regeneration [65]. For allogenic cartilage applications, Zhang et al. (2023) developed a curcumin-loaded PLGA nanofibrous membrane to protect engineered cartilage by creating a localized immunosuppressive environment as this membrane was explicitly designed to release curcumin gradually, which helped to reduce the production of inflammatory cytokines such as IL-1β, IL-6, and TNF-α in macrophages; hence, this downregulation limited the immune response in the surrounding tissue. This immunomodulatory scaffold was tested in a rat cartilage defect model, and it was observed that the membrane encapsulated the allogenic cartilage implant, preserving it. Two weeks' post-implantation, this curcumin-releasing membrane maintained cartilage integrity, reduced local inflammation, and supported cartilage repair, while in the PLGA-only and pure cartilage (non-encapsulated) groups, the cartilage exhibited a higher inflammatory response and more significant degradation [66]. Similarly, Huo et al. (2023) engineered a semi-permeable thermoplastic polyurethane/gelatin (TPU/GT) electrospun membrane to achieve immunoisolation, ensuring stable cartilage regeneration. This semi-permeable membrane effectively shielded the transplanted cartilage from immune cells in a goat model, showing reduced immune factor production and stable regeneration, marking these as promising clinical cartilage transplantation strategies [67].

Other researchers suggested using GT-added nanofibers as an interesting preclinical model to explore the effect of drugs and chemotherapeutic administration after damaged muscle resection [68]. They investigated the in vitro response of human mesenchymal stem cells (hMSCs) on PCL-based fibers in the presence of 5-azacytidine to evaluate how the fibrous network may influence the drug's therapeutic effect during in vitro myogenesis. They demonstrated that electrospun fibers could support 5-azacytidine's capability to reduce the proliferation rate of hMSC, thus promoting hMSC differentiation into mature myofibers when conditioned in supplemented myogenic media.

Abdulmalik et al. (2023) explored a PCL–cellulose acetate scaffold with Exendin-4-loaded halloysite nanotubes for sustained bioactive release in tendon regeneration. This scaffold fostered tenogenic differentiation and upregulated tendon-specific genes in hMSCs. Applied in a rat Achilles tendon injury model, it reduced fibrocartilage formation and promoted tendon healing [69]. Iorio et al. (2024) complemented this approach with an aligned PCL/PGS (poly-glycerol sebacate) scaffold, supporting stem cell adhesion and teno-differentiation, showing promise for tendon TE with relevance for ligament repair [70].

Electrospun scaffolds also deliver gene therapy systems to enhance tissue regeneration. Recently, Liu et al. (2024) developed an advanced dual-layer electrospun membrane explicitly designed for the targeted delivery of COX-2 siRNA to reduce tendon adhesions, as they can severely impair tendon mobility and function. This membrane comprised a

positively charged outer layer of PCL and chitosan, facilitating unidirectional gene delivery through charge repulsion. In vitro studies confirmed that this setup controlled the release of COX-2 siRNA, successfully reducing fibroblast proliferation, which is a critical factor in preventing tendon adhesions. In a rat Achilles tendon injury model, the membrane decreased tendon adhesions, reduced inflammation, and improved tendon healing [71].

These findings underscore electrospun scaffolds' potential in targeting cartilage, tendon, and ligament tissue regenerative needs, leveraging bio-factors' release, immunomodulation, and controlled structural alignment to foster effective tissue repair and regeneration.

#### 3.1.5. Central and Peripheral Nerves

Electrospun scaffolds are increasingly used to support peripheral nerve regeneration by incorporating materials that enhance electrical conductivity and cellular compatibility. For instance, Xiong et al. (2023) created a biomimetic, piezoelectric, and conductive aligned electrospun scaffold using polypyrrole (PPy), polydopamine (PDA), and PLLA. This composite scaffold aimed to improve the hydrophilicity and cellular compatibility of PLLA while maintaining a robust piezoelectric effect to promote Schwann cell differentiation and dorsal root ganglion neuron alignment. In vivo, the aligned PPy/PDA/PLLA scaffold bridged a 10 mm sciatic nerve gap, promoting axon alignment, myelination, and functional recovery by activating calcium and AMP-activated protein kinase pathways, yielding nerve regeneration, which can be compared to autografts [72]. Similarly, Wei et al. (2024) also explored the potential of electroactive and aligned PPy/PDA/PLLA fibers in guiding MSCs into *Schwann-like* cells. In a rat sciatic nerve defect model, this scaffold effectively enhanced nerve regeneration, myelination, and functional recovery in 12 weeks [73]. Also, Ma et al. (2024) produced electrospun PCL and polyaniline (PANI) conductive fibers that supported Schwann cell adhesion and proliferation, critical for effective nerve repair. This scaffold was also tested in a rat sciatic nerve defect model, and its fibers enhanced axon diameter, improved walking scores, and facilitated functional recovery, demonstrating the benefits of integrating conductive properties into nerve scaffolds [74]. Furthermore, Puhl et al. (2023) developed an innovative electrospun scaffold using PLLA fibers coated with dextran sulfate sodium (DSS) and polydopamine (pDOPA) to facilitate the localized delivery of neurotrophin-3 mRNA to promote neurite growth by significantly increasing NT-3 secretion from Schwann cells, a critical factor for nerve regeneration as it plays a critical role in promoting the extension and alignment of neurites, facilitating the reconnection of damaged nerve fibers [75]. This scaffold acted as a structural framework and a localized delivery platform pivotal for nerve regeneration.

Moreover, Pires et al., [76] proposed the fabrication of electrospun fibers made of poly (trimethylene carbonate-co-ε-caprolactone) [P(TMC-CL)] loaded with a non-steroidal anti-inflammatory drug—i.e., ibuprofen—as a drug delivery system able to limit the inflammatory response and support axonal regeneration in the presence of spinal cord lesions. All of the proposed systems showed a full release of ibuprofen in 24 h, under physiological conditions, by a diffusion-dependent kinetic mechanism. Some differences in terms of burst release occurred as a function of fiber diameter distribution. However, in all cases, biological activity related to the release of prostaglandin E2 was reduced when human-derived macrophages were incubated in the presence of ibuprofen, thus confirming the therapeutic effect of drug delivery on the biological response.

Another innovative approach by Mao et al. (2023) involved a bilayered nerve conduit combining a PLA-PCL outer layer with a biologically active inner layer made from a porcine-derived extracellular matrix. The PLA-PCL layer provides mechanical stability and protection, making the conduit structurally robust for implantation. In contrast, the ECM inner layer serves as a bioactive environment that closely mimics the biochemical

composition of native nerve tissue. When tested in a 10 mm rat sciatic nerve gap model, the bilayer scaffold improved outcomes over a scaffold made solely of PLA-PCL. The results showed enhancements in Schwann cell activity and axonal growth, facilitating nerve function recovery [77].

Each of these studies highlights the versatility and efficacy of electrospun scaffolds in tissue engineering. They are used for both hard and soft tissue applications with materials that facilitate cell attachment, promote essential biochemical signaling, and support structural alignment, all of which are pivotal for effective organ regeneration or repair. Accordingly, Table 1 collects recent findings of electrospinning applications in TE.

**Table 1.** Recent advances of electrospun scaffold applications in tissue engineering: fiber characteristics and findings.

| Tissue | Composition/Solvents | Fiber Diameter | Key Findings | Ref. |
|---|---|---|---|---|
| Bone | -PLGA/PCL with linezolid<br>-Solvent: HFIP | -PLGA: 930 ± 150 nm<br>-PLGA/PCL with linezolid: varying diameters | -Effective methicillin-resistant *S. aureus* control in vitro and in vivo<br>-Effective localized infection control for prosthetic applications | [47] |
| | -PLA with bioactive glass (n-BG) and MgO<br>-Solvent: DCM and DMF | -PLA-only: 1.7 ± 0.6 µm<br>-PLA/n-BG/n-MgO: 2.8–3.1 µm | -Increased HA formation<br>-Antimicrobial activity against *S. aureus*<br>-Elevated ALP expression in osteoblast cells | [46] |
| | -PLLA/PCL with 58S bioactive glass<br>-Solvent: DCM and DMF | 1.5 µm | -Enhanced cell proliferation (Saos-2 cell line)<br>-Compressive modulus 6.1 ± 0.4 kPa<br>-Pore size ~335.3 µm | [43] |
| | -GT/PVA/SF with Cu-HAP<br>-Solvent: Double-distilled water and acetic acid | Not reported | -Antimicrobial activity<br>-High porosity (99%); hemolysis <5%<br>-ALP activity increases over 7–14 days | [44] |
| | -PCL, UCNPs, MgO<br>-Solvent: HFIP | PCL: 1.78 µm, PCL-UCNPs-1%MgO: 1.65 µm | -Enhanced ALP activity<br>-Bone regeneration in rat skull defects<br>-Scaffold degradation tracked non-invasively | [48] |
| | -PCL blended with starch and 5% CaO<br>-Solvent: Formic acid | -PCL/starch/CaO: 750 ± 120 nm | -Bioactivity and controlled scaffold<br>-Promoted HA formation<br>-Increased Young's modulus | [45] |
| | -Gelatin–PCL blend with nHAp;<br>-Solvents: Acetic acid and chloroform/methanol | -Gelatin-PCL-nHAp: 615 ± 269 nm | -Improved osteoblast adhesion and proliferation<br>-Cells exhibited healthy morphology<br>-Increased mechanical strength | [78] |
| | -PCL with collagen type I (19:1 ratio)<br>-Solvent: TFE | -PCol: 390 ± 71 nm<br>-PCL-only: 804 ± 186 nm | -Increased wettability and cell adhesion<br>-Promoted organized skin regeneration in normal skin morphology in vivo<br>-PCL/collagen/hWJ-MSC supported cell adhesion and regeneration | [51] |

**Table 1.** *Cont.*

| Tissue | Composition/Solvents | Fiber Diameter | Key Findings | Ref. |
|---|---|---|---|---|
| Skin | -PLA with phenytoin, sildenafil citrate, and simvastatin<br>-Solvent: Acetone, acetic acid, and DCM | 709 ± 178 nm | -Sustained drug release and high biocompatibility<br>-Promoted complete re-epithelialization, organized cell layers, and no scar tissue after 21 days in vivo | [56] |
| | -PU and starch/hyaluronic acid<br>-Solvent: DMSO and DMF | 428 ± 78.32 nm | -Enhanced cell attachment and proliferation<br>-Improved wound healing with organized tissue structure in vivo | [79] |
| | -SEFM is composed of polyglactin 910 and polydioxanone<br>-Solvent: Not specified | Not specified; matrix designed to mimic human ECM | Clinical trial: 74% of diabetic foot ulcer patients achieved 100% re-epithelialization in 12 weeks, vs. 33% in standard care | [57] |
| | -PVP/PVA<br>-Solvent: ethanol and 90% acetic acid | 150–400 nm | -Non-toxic to fibroblasts, low hemolysis<br>-In vivo slow degradation and minimal inflammation in rats | [49] |
| | -Silk fibroin and gelatin with propolis (SF/GT-EP)<br>-Solvent: formic acid | SF/GT-1%EP: 200–400 nm | -Enhanced fibroblast cell migration<br>-Promoted wound healing and re-epithelialization in mice | [54] |
| | -PU, PRGF, and gelatin with *L. plantarum*<br>-Solvent: THF, DMF | 516 ± 147 nm | -Supported cell proliferation<br>-Antibacterial potential<br>-Improved wound healing, angiogenesis, and reduced infection in a rat model | [53] |
| | -CS and polyethylene oxide with cerium oxide nanoparticles<br>-Solvent: 70% acetic acid | 175 ± 76 nm | -High MSC compatibility, supported cell growth<br>-Good tissue integration, slow degradation, minimal inflammation in vivo | [55] |
| | -PCL and PEG supplemented with egg yolk oil<br>-Solvent: DCM: DMF (9:1) | 191 ± 61 nm | -Enhanced fibroblast cell viability and antibacterial properties<br>-Promoted wound healing, re-epithelialization, and collagen synthesis | [50] |
| | -PLGA with curcumin<br>-Solvent: Trichloromethane | Not specified; nanoscale structure confirmed by SEM | -Sustained curcumin release and reduced inflammation<br>-Rat cartilage defect model showed immunosuppressive effects and cartilage preservation | [66] |
| | -PCL and silk fibroin<br>-Solvent: HFIP<br>(R: Randomly oriented, A: Aligned) | -RPCL 552.4 ± 189.8 nm<br>-RPCL/SF 423.6 ± 199.4 nm<br>-APCL/SF 361.9 ± 151.3 nm | -APCL/Silk fibroin nanofibers promoted articular chondrocyte proliferation and type II collagen gene expression<br>-Promoted the elongation of articular chondrocytes in the direction of parallel fiber alignment | [80] |
| | -PLLA with barium titanate (BT) infused with FGF-18<br>-Solvent: HFIP | Not specified; scaffold morphology assessed via SEM | -Enhanced chondrocyte proliferation and cartilage-related gene expression<br>-Cartilage regeneration and ECM remodeling | [65] |

**Table 1.** *Cont.*

| Tissue | Composition/Solvents | Fiber Diameter | Key Findings | Ref. |
|---|---|---|---|---|
| Cartilage and tendon | Thermoplastic polyurethane and gelatin<br>-Solvent: HFIP | 0.31 ± 0.06 µm | -Biocompatible and semi-permeable; blocks immune cell infiltration<br>-Goat model showed stable allogeneic cartilage regeneration without immune rejection | [67] |
| | -PCL and chitosan<br>-Solvents: HFIP, formic acid, and acetone, respectively | siRNAGP/CSPCL scaffold ± 0.06 µm | -Controlled COX-2 siRNA release, reducing fibroblast proliferation<br>-Reduced inflammation and better healing in a tendon model | [71] |
| | -PCL/Cellulose acetate<br>-Solvent: TFE | 600–1000 nm | -Supported hMSC proliferation and tendon gene expression.<br>-Promoted tendon healing and functional recovery in a tendon model | [69] |
| | -PCL/PGS<br>-Solvent: acetic acid | 1.01 ± 0.44 µm. | -Supported amniotic epithelial stem cells adhesion, growth, and teno-differentiation | [70] |
| Cardiac and vascular | -GT/PCL<br>-Solvent: Chloroform | 1.02 ± 0.13 µm | -High mechanical integrity enhanced endothelial cell viability<br>-Good hemostatic performance and patency in the swine pulmonary artery model | [58] |
| | -SF/fibroin<br>-Solvent: Formic acid | SF/fibroin (25:75)<br>424 ± 11 nm | -Enhanced mechanical strength and MSC proliferation<br>-Faster degradation and tissue regeneration in the rat model | [81] |
| | -PLGA core and PCL shell<br>-Solvent: HFIP | HCS1508 scaffold (best tensile properties):<br>2.05 ± 0.60 µm | -Strong mechanical properties, improved degradation in vitro<br>-Stable endothelialization, low inflammation, and no calcification at 12 months in rat aorta | [59] |
| | -PCL and placental extracellular matrix (pECM),<br>-Solvent: HFIP | PCL-epECM/H-IL-4<br>7.4 ± 1.3 µm | -Promoted macrophage anti-inflammatory polarization and endothelial cell proliferation<br>-Enhanced endothelialization and smooth muscle regeneration in rat artery model | [63] |
| | -5% Carbothane™ 3575A with 10% GT<br>-Solvent: HFIP | 0.39 ± 0.11 µm | -Improved cell adhesion and endothelial compatibility<br>-Superior patency and compatibility compared to expanded polytetrafluoroethylene grafts in the Wistar rat aorta model | [64] |
| | -PCL/Polydioxanone, PLCL, PLGA<br>-Solvent: Chloroform and HFIP | PLCL/Polydioxanone (best-performing scaffold):<br>1.76 µm (prior to stent expansion) | -High stretchability and hemocompatibility except for polydioxanone<br>-PLGA failed in 1 day; PCL and PLCL exhibited good biocompatibility and biodegradation in the rat aorta model | [82] |

**Table 1.** *Cont.*

| Tissue | Composition/Solvents | Fiber Diameter | Key Findings | Ref. |
|---|---|---|---|---|
| | -PCL, SF, CNTs with brown adipose-derived stem cell sheets<br>-Solvent: HFIP | PCL/SF<br>1.156 ± 0.296 µm | -Promoted cardiomyogenic differentiation and electrical conductivity<br>-Enhanced angiogenesis, reduced inflammation, and supported cardiomyocyte regeneration in rat myocardial infarction model | [60] |
| | -PU with salvianolic acid A<br>-Solvent: HFIP | 1.33 ± 0.174 µm. | -Anti-inflammatory, angiogenic gene expression, reduced inflammatory cell chemotaxis<br>-Improved myocardial recovery and re-endothelialization in myocardial infarction and arterial repair rat models | [70] |
| | -PLA, PLGA loaded with dexamethasone<br>-Solvent: TFE and chloroform | PLA:<br>317.38 nm ± 82.57 nm.<br>PCL:<br>342.72 nm ± 56.27 nm | -Sustained dexamethasone release over 50 days, promoting cell adhesion | [83] |
| | -PCL with ascorbic acid (AA)<br>-Solvent: HFIP | PCL—0.3%AA:<br>1.88 ± 0.14 µm | -Reduced reactive oxygen species and oxidative stress<br>-High cytocompatibility with human umbilical vein endothelial cells | [62] |
| Nerve | -PLLA with PPy and PDA<br>-Solvent: HFIP | PPy/PDA/PLLA:<br>3.60 ± 0.20 µm,<br>PDA/PLLA:<br>3.46 ± 0.29 µm, PLLA:<br>2.81 ± 0.15 µm | -Enhanced nerve cell attachment and axonal alignment<br>-Rat sciatic nerve model showed improved myelination and functional recovery | [72] |
| | -PCL and porcine-derived nerve ECM<br>-Solvent: TFE | 886.09 ± 185.43 nm | -Supported Schwann cell adhesion and proliferation<br>-Rat sciatic nerve model demonstrated biocompatibility, improved nerve regeneration, and functional recovery | [74] |
| | -PLLA coated with DSS and pDOPA<br>-Solvent: Chloroform | -Uncoated PLLA:<br>1.98 ± 0.38 µm<br>-2pDOPA coated:<br>1.96 ± 0.20 µm | -Enhanced Schwann cell NT-3 secretion with the pDOPA functionalized scaffold<br>-Supported increased neurite extension from dorsal root ganglia | [75] |
| | -PLA-PCL outer layer, porcine-derived nerve ECM inner layer<br>-Solvent: Acetic acid | -PLA-PCL layer thickness:<br>0.121 mm ± 0.010<br>-ECM layer:<br>0.104 mm ± 0.008<br>-Scaffold inner diameter:<br>1.342 mm ± 0.025 | -High biocompatibility, cell affinity, retention of bioactive molecules (collagen, laminin, and fibronectin, etc.)<br>-Rat sciatic nerve gap model showed superior nerve regeneration compared to PLA-PCL alone | [77] |

**Table 1.** *Cont.*

| Tissue | Composition/Solvents | Fiber Diameter | Key Findings | Ref. |
|---|---|---|---|---|
| | -PPy, PDA, PLLA<br>-Solvent: TFE | ~5 µm | -MSC differentiation was promoted into Schwann-like cells, as indicated by increased markers<br>-Enhanced nerve regeneration, myelination, and functional recovery in rat sciatic nerve model | [73] |
| | -PLA with lithium<br>-Solvent: Chloroform and DMF (4:1) | ~550 nm | -Scaffold-enhanced Schwann cell marker expressions and differentiation of human adipose-derived mesenchymal stem cells<br>-Lithium-loaded scaffold facilitated Schwann cell differentiation and improved sensory and motor functions in vivo, with well-organized myelinated axons | [84] |
| | -PCL/GT with heparin and growth factors<br>-Solvent: HFIP | -Inner side fiber diameter:1.49 ± 0.51 µm and<br>-Outer: 1.89 ± 0.70 µm | -Heparin-immobilized PCL/gel with neural growth factor and basic fibroblast growth factor retained bioactivity and facilitated nerve regeneration, reducing inflammatory infiltration in vivo | [85] |

Solvent abbreviations: HFIP—hexafluoroisopropanol; TFE—trifluoroethanol; DCM—dichloromethane; DMF—dimethylformamide; THF—tetrahydrofuran; TFE—trifluoroethanol.

## 4. Basics of 3D-Printing Technology and Its Application in Tissue Engineering

Three-dimensional printing is a process in which a 3D physical object is created from a virtual model, file, or electronic source. The creation of an object through 3D printing is based on carefully adding material layer by layer to develop the parts of the object, which is why 3D printing is commonly referred to as additive manufacturing (AM). The main components of a 3D-printing process are as follows: (1) The design of the tailored 3D object to print, which is saved into an STL (Standard Tessellation Language) file and then goes to a "slicer" software to create (2) a g-code file; this type of file is the instruction that the printer will read. (3) The 3D printer then develops the object by adding a material layer over another in a gradual and controlled way [86–88]. Figure 3 shows the workflow of a 3D-printing process. While these three components are the essentials in 3D printing, it is important to mention that there are several 3D-printing techniques. Some of the main methods and their principles will be addressed in subsequent sections, and recent reports on 3D printing in TE are shown in Table 2.

**Table 2.** Three-dimensional printing technology applications in tissue engineering: scaffold characteristics and findings.

| Method | Materials | Scaffold Characteristics | Application and Findings | Refs. |
|---|---|---|---|---|
| Fused Deposition Modeling | PLA with 30% HA powder | Cubic, cylindrical, and hexagonal porous structures with pore sizes of 0.8 and 1.2 µm, compressive strength 5.5–7.5 MPa | Cubic structure had maximum permeability; hexagonal structure enhanced apatite formation, promoting bioactivity | [89] |
| | Pure PLA filament | Gyroid structure with unit cell sizes of 2, 2.5, and 3 mm, pore sizes 1.3, 1.7, and 2 mm, porosity 86–90%, compressive strength up to 180 MPa | Gyroid structure exhibited high mechanical strength and anisotropy, making it suitable for bone tissue applications | [90] |

**Table 2.** *Cont.*

| Method | Materials | Scaffold Characteristics | Application and Findings | Refs. |
|---|---|---|---|---|
| Stereolithography | Elastic resin with lidocaine hydrochloride | Hollow and solid elastic devices; 0.5 mm shell for hollow, flexible for bladder retention | Hollow devices released lidocaine over 4 days; solid devices extended release up to 14 days; high flexibility suitable for bladder retention | [91] |
| | Poly-trimethylene carbonate (PTMC) with HA nanoparticles | Gyroid structure, 70% porosity, minimum pore size of 600 µm, HA-enriched surface | HA-enriched surfaces promoted cell attachment, differentiation, and mineralization; PTMC/HA scaffolds showed improved bone ingrowth and integration | [92] |
| | Ti6Al4V alloy (20–50 µm powder) | Hierarchical micro/submicron texture created by acid etching; dimensions: 10 × 10 × 2 mm (in vitro), 2 × 3 mm cylinders (in vivo); rougher than SLA surface | Osteogenic application: in vitro MSCs adhesion, proliferation, differentiation) and in vivo (osseointegration in rat femoral condyle) | [93] |
| Selective Laser Sintering | PCL with HA | Circular discs, 15 mm diameter, 1 mm thickness, interconnected pores, HA distributed within PCL matrix | Optimized SLS conditions improve scaffold stability; HA promoted cell adhesion and apatite formation | [94] |
| | PCL powder | Square pyramid unit cells, 85% porosity, micropores of 40–100 µm, tensile stiffness 0.43 MPa, compressive stiffness 345 kPa | Scaffold architecture supports cardiac cell colonization and differentiation, maintaining viability over 21 days | [95] |
| | PVA powder | Tetragonal structure with interconnected pores, 67.9% porosity, and pore size controlled via SLS settings | Stable, porous scaffolds for nutrient and waste exchange; MG-63 cells adhered and proliferated, confirming biocompatibility | [96] |
| Digital Light Processing | HA powder with photopolymer resin and liquid sodium polyacrylate | 300–600 µm pore size, 49.8% porosity, compressive strength 15.25 MPa | Supported cell adhesion, proliferation, and differentiation; high precision and biocompatibility for bone TE | [97] |
| | Zirconia ($ZrO_2$) and HA composite in photosensitive resin | Porosity 54.6%, shrinkage 23–28% post-sintering, compressive strength 20 MPa | HA addition improved bioactivity; optimal mechanical properties at 10 wt% HA for bone TE | [98] |
| | Calcium phosphate powders with monoalcohol ethoxylate phosphate in photosensitive resin | Three designs (cube, octet-truss, inverse fcc); inverse fcc has the highest porosity and compressive strength | Macropore geometry influenced osteogenic properties; inverse fcc showed enhanced osteoinduction | [99] |
| Selective Laser Melting | Commercially pure titanium | Gyroid design, 68–73% porosity, unit cell sizes of 2, 2.5, and 3 mm; compressive strength 44.9 to 56.5 MPa | High compatibility with bone elastic modulus; ductility up to 50% strain; optimized roughness for bone integration | [100] |
| | Titanium alloy (Ti6Al4V) | Gyroid microarchitecture, 50–90% porosity, unit cell sizes 4 mm and 6 mm; wall thicknesses 0.25, 0.5, and 1.0 mm | Improved fatigue resistance with thicker walls, optimal laser parameters, and enhanced integrity for bone repair | [101] |
| | Ti6Al4V alloy with chitosan-wollastonite nanoparticles. | Porous structure, 48–52% porosity; 10 wt% WS-NPs showed the highest compressive strength of 420 MPa | Chitosan–wollastonite improved bioactivity and mechanical strength, has low cytotoxicity, and is promising for orthopedic use | [102] |
| Laminated Object Manufacturing | Biodegradable poly(lactic) acid (PLA) | Laminated object manufacturing technique; infill patterns (linear, triangular, honeycomb); infill densities (50–90%); disc thickness (3.4–5.6 mm) | Intended for marine and structural engineering applications; best performance observed with honeycomb infill pattern at 70% density, achieving a compressive strength of 42.47 MPa; highlighted the significance of the infill pattern and number of discs in enhancing mechanical properties | [103] |
| Melt-electrowriting | Polycaprolactone (PCL), gelatin methacryloyl (GelMA), chondroitin sulfate methacryloyl (ChsMA) | Anisotropic scaffolds made by MEW combined with bioactive hydrogels | Intended for pediatric heart valve tissue engineering; improved hemocompatibility and endothelialization; reduced immune reaction and calcification in vivo | [104] |
| | PCL | A bilayered scaffold made by MEW mimics conjunctival stromal and epithelial layers | Used for ocular surface reconstruction; supported growth of conjunctival stromal and epithelial cells; no in vivo assessments mentioned | [105] |
| | PCL, HA, and Roxithromycin (ROX) | Composite scaffold combining MEW and SES techniques contains microfibers and nanofibers with embedded HAP and ROX | Aimed at bone tissue engineering, enhanced osteogenic differentiation, and antibacterial properties; significant bone formation observed in vivo | [106] |
| | Low-molecular-weight PCL, and HA nanoparticles | The scaffold was made using melt-electrowriting with high HA concentration | Designed for bone tissue regeneration, higher metabolic activity, and osteogenic markers; no in vivo results were reported | [107] |

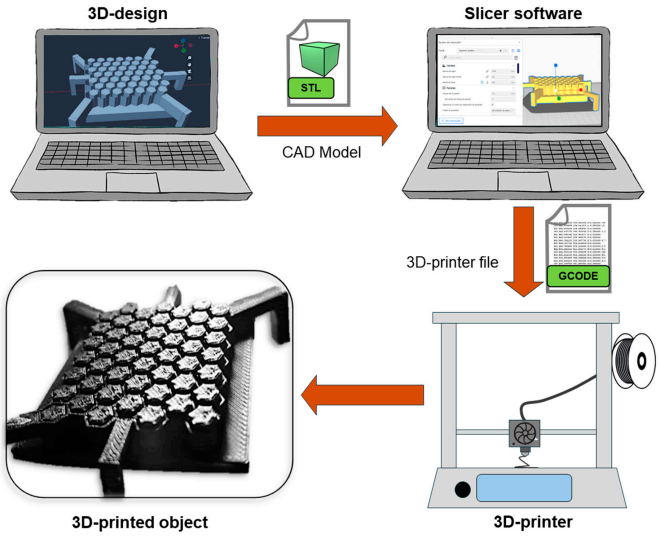



**Figure 3.** Schematic illustration of the 3D-printing process.

### *4.1. Fused Deposition Modeling*

Fused deposition modeling (FDM) is a 3D-printing process where material, typically a thermoplastic filament, is heated to a semi-liquid state and precisely deposited layer by layer to produce the desired structure. As mentioned above, FDM is controlled by a computer-aided design (CAD) program, which directs the nozzle's movements to create each layer according to the specified contours and design. In FDM, it is crucial to consider that the strength and quality of FDM-printed parts depend on several factors, including material type, layer configuration, and specific printing parameters like speed, temperature, and infill density [108,109]. Known also as Fused Filament Fabrication (FFF), in FDM, the primary material used is a filament, typically composed of a pure polymer with a relatively low melting point, for example, PLA, acrylonitrile butadiene, and polypropylene. However, researchers and industries have developed composite filaments to improve or tailor the design properties, such as mechanical strength, conductivity, and thermal resistance. These composite filaments are produced by blending a base polymer with reinforcing agents, such as carbon fibers, glass fibers, metal powders, or nanoparticles. This tailoring of materials allows for more versatile applications, providing printed products with specific attributes suitable for advanced prototyping, functional parts, or even end-use products [110].

### *4.2. Stereolithography*

Stereolithography (SLA) is a 3D-printing process that builds objects by curing thin layers of liquid resin with a UV laser through a technique known as photopolymerization. The laser selectively solidifies each layer based on a predefined pattern, and as each layer cures, the platform lowers incrementally to allow fresh resin to coat the surface. This controlled layer-by-layer approach enables SLA to produce intricate and highly detailed parts, following precise cross-sectional designs until the complete 3D structure is formed [111,112].

SLA relies heavily on photopolymer resins, which harden when exposed to UV light, allowing for the precise layer-by-layer construction of 3D objects. Typical resins used in SLA include acrylate-based polymers and methacrylate resins, which provide good dimensional stability, fine detail, and smooth surface finishes. Advanced SLA applications have incorporated biocompatible and biodegradable resins for medical use, flexible resins for wearable devices, and high-strength composites that add functionality to complex designs in automotive and aerospace fields. SLA is notably used for applications demanding

high resolution and fine details, such as dental models, hearing aids, intricate molds, and investment casting patterns [113,114].

### 4.3. Selective Laser Sintering (SLS)

Selective Laser Sintering (SLS) is an advanced AM technique that constructs 3D objects from powdered materials using laser energy to fuse particles layer by layer. As a type of powder bed fusion, SLS relies on a high-power laser to scan and selectively melt regions on the surface of each powder layer, causing the particles to melt and bond together partially. Once a layer is completed, the build platform lowers slightly, allowing the spreading system to deposit a new powder layer, which is then selectively fused by the laser according to the design. This cycle continues until the final 3D structure is produced based on CAD specifications [115,116]. One advantage of SLS is its ability to produce complex geometries with high resolution without requiring additional solvents, binders, or support structures, which are often necessary for other 3D-printing methods. Additionally, SLS allows the recycling of unused powder, improving the process. This method is often used to manufacture parts in sectors that demand durability and complexity, such as aerospace, automotive, and medical industries, as well as for pharmaceutical applications where drug stability and safety are critical [117].

### 4.4. Digital Light Processing

Digital Light Processing (DLP) is an AM technology that constructs parts layer by layer using a projected light source to cure photosensitive resin. Unlike other methods that cure point by point, DLP operates with a digital micro-mirror device (DMD) to project an entire 2D layer image simultaneously, rapidly solidifying it in precise alignment with the previous layers. Each projection uses micro-mirrors to create a pattern of light and dark pixels, which defines the layer's resolution and accurately shapes each cross-section. The printing platform adjusts vertically, either in a "top-down" or "bottom-up" configuration, to allow the object to form continuously as each new layer is added [118,119].

DLP technology may incorporate basic photopolymer resins and ceramic and metal-loaded suspensions, which allow the production of components that can undergo debinding and sintering. This advancement opens applications beyond traditional polymers, making DLP valuable for industries needing detailed resolution and the versatility of different material options. Technology's efficiency and adaptability make it suitable for applications ranging from intricate dental and medical models to durable parts requiring post-processing [120].

### 4.5. Selective Laser Melting

Selective Laser Melting (SLM) is an AM technique using a high-power ytterbium fiber laser to melt and fuse metallic powders into complex, three-dimensional components. Like SLS, SLM relies on layer-by-layer construction based on a CAD model. However, unlike SLS, SLM fully melts the material, achieving nearly 100% density and creating robust, net-shape parts with high precision. The process starts by distributing a thin layer of metallic powder across a build platform, which is then scanned by the laser to melt selected areas. This cycle repeats layer by layer, allowing for precise fusion and strong interlayer bonding until the final component is complete [121,122].

SLM can work with various metals, including aluminum, magnesium, and titanium alloys, and is valued in industries where complex, strong metal parts are needed, such as aerospace and medical implants. Though traditionally metal-focused, certain ceramic materials, like zirconia, can also be used. Despite advancements in SLM, the limited availability of compatible materials remains a challenge. However, the technology's ability

to produce near-full-density parts and high-detail geometries makes it a vital tool for high-performance applications where component integrity and durability are essential [122,123].

### *4.6. Laminated Object Manufacturing*

Laminated object manufacturing (LOM) is a layer-based AM technique where 3D objects are constructed by the sequential bonding and cutting of thin sheets of material, such as paper, metal, or ceramics, according to CAD-driven contours. In the LOM process, a laser or blade cuts each sheet layer to a cross-sectional shape, which is then adhered to the previous layers. This layered approach is repeated, enabling the creation of complex shapes with minimal material waste. A heated roller is typically used to apply pressure, facilitating the bonding of layers, while uncut areas are removed, simplifying the formation of internal geometries [124,125].

Standard LOM materials include adhesive-coated paper, plastics, and metal laminates, with ceramic-loaded tapes used for applications requiring high durability and thermal resistance. However, objects often exhibit a "stair-step" effect on angled surfaces due to the stacking of layers, which can be adjusted based on the material and layer thickness. LOM is particularly advantageous for rapid prototyping, pattern making, and applications in the automotive and aerospace industries, where durable and complex shapes are required efficiently [126].

### *4.7. Melt Electrowriting*

Melt electrowriting (MEW), introduced in 2011, represents a significant advancement in additive manufacturing. This technique combines thermal polymer extrusion with electrospinning principles to precisely deposit continuous polymeric microfibers by applying an electric field to draw a molten polymer from a spinneret toward a computer-controlled collector plate, either planar or rotating. The coordination between the collector's movement and the polymer jet allows for structured fiber deposition, facilitating the creation of complex three-dimensional scaffolds [127,128].

In TE, MEW is particularly effective in creating personalized scaffolds that closely mimic the complexity and function of native tissues. Its ability to generate highly porous structures with micro- to nanoscale resolution surpasses traditional methods like FDM, which often needs improvements in resolution, and solvent-based electrospinning, which struggles with fiber orientation and solvent evaporation. Utilizing CAD and rotating collectors, MEW constructs structurally complex tubular scaffolds tailored for TE applications. Its precise control over the scaffold architecture, ranging from simple geometric patterns to biologically mimetic structures, makes MEW particularly effective in fabricating tissue-specific ECM-like scaffolds and adapting to various pathophysiological conditions [129–131]. However, while MEW offers the advantage of creating highly controlled scaffold shapes with fiber diameters ranging from about 3 to 22 μm, it does not achieve the exact resolution of electrospinning [131]. Electrospinning can produce fibers with diameters spanning from a few nanometers to several micrometers, allowing for even finer structures. This finer resolution is advantageous in applications requiring dense, highly detailed fibrous networks, such as in advanced TE and filtration systems [132].

One of the most common materials in MEW is PCL due to its favorable properties, such as its relatively low melting point, rapid solidification, and excellent biocompatibility. These characteristics make PCL ideal for creating constructs that require precise control over fiber diameter, pore size, and overall 3D architecture. Other polymers, PP, photocurable poly (l-lactide-co-ε-caprolactone-co-acryloyl carbonate), and water-soluble poly(2-ethyl-2-oxazoline) have also been utilized to expand the applications of MEW in creating functional and structurally diverse scaffolds [129,132].

## 5. Combining Electrospinning and 3D Printing

The combination of 3D printing and electrospinning represents a valuable strategy for creating complex, functional scaffolds in TE. While 3D printing enables the design of custom-shaped scaffolds with interconnected pores that facilitate nutrient transport, it lacks the high resolution needed to mimic the finer structures of native tissues and typically produces pore sizes larger than cells, which can impede cell seeding and tissue integration. Moreover, its limited material choices and inability to create nanoscale surface features restrict its capacity to mimic ECM. Conversely, electrospinning generates nanofibers that closely resemble the ECM, offering abundant sites for cell attachment and promoting cell growth. These fibers can also deliver bioactive molecules, supporting tissue regeneration through controlled release. However, electrospun scaffolds often lack the mechanical strength and controlled shaping required for more robust applications [9,10].

Integrating these two techniques combines the mechanical stability and customizability of 3D printing with the biomimetic nanostructure of electrospinning, yielding scaffolds with enhanced cell-supportive properties and a broader range of material options. This hybrid approach thus provides a versatile platform for creating specialized, high-performance scaffolds tailored to specific TE needs. This section will discuss the different methods for combining 3D printing and electrospinning (illustrated in Figure 4).

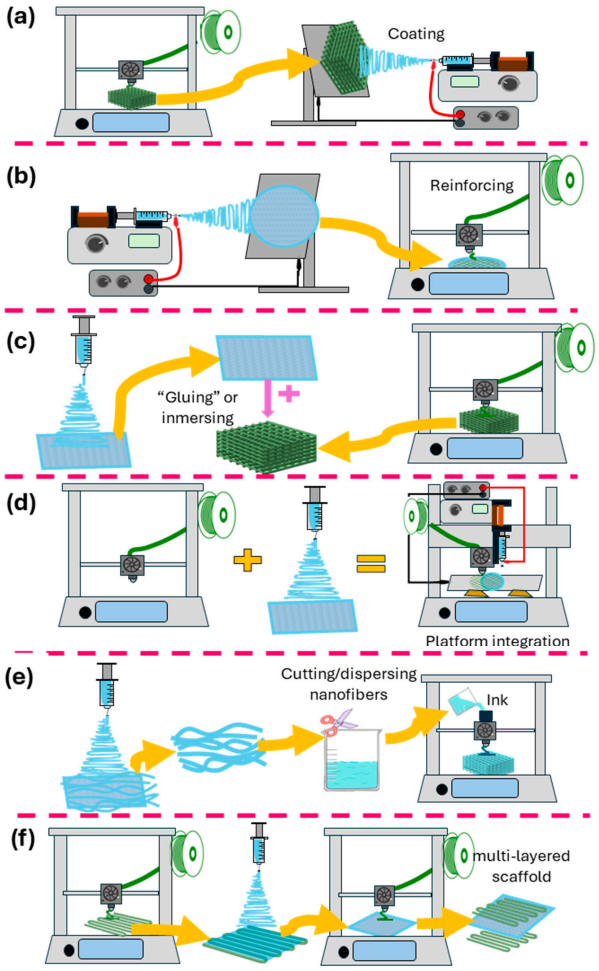



**Figure 4.** Schematic representation of the different methods for combining 3D printing and electrospinning. (**a**) Electrospinning onto 3D-printed scaffolds. (**b**) 3D printing onto electrospun fibers. (**c**) Decorating/infusing 3D-printed scaffolds with electrospun nanofiber segments. (**d**) Platforms combining 3D-printing and electrospinning techniques. (**e**) Electrospun fibers are used as inks for 3D printing. (**f**) Alternate use of 3D printing and electrospinning.

### *5.1. Electrospinning onto 3D-Printed Scaffolds*

Combining 3D-printing and electrospinning techniques using electrospinning onto pre-printed 3D scaffolds has demonstrated remarkable potential in TE applications by enhancing mechanical and biological properties across various scaffold designs. In this process, an initial scaffold is created using 3D printing—often via fused deposition modeling—to produce a defined, often porous structure that offers a customizable base. Once the 3D structure is printed, electrospun fibers are deposited onto the scaffold, forming a layered or embedded fiber matrix that closely mimics the extracellular matrix. This dual-layer design allows researchers to directly introduce materials with specific mechanical or biological functions onto the printed framework. For example, Farsi et al. (2022) developed a PLA scaffold using FDM, which was subsequently coated with electrospun polyvinyl alcohol (PVA) and hyaluronic acid (HLA) fibers. This composite design increased mechanical properties such as the elastic modulus and tensile strength and promoted enhanced cell adhesion and proliferation when tested with rabbit chondrocytes [133]. Similarly, Kurowska et al. (2023) employed a 3D-printed PCL scaffold layered with bioglass and Zn-doped bioglass, followed by a PCL-OST electrospun membrane, which improved cell viability and proliferation, supporting cartilage regeneration by promoting collagen type II secretion in knee chondrocytes [134].

Similarly, Araya et al. optimized the fabrication of PLA-based composites by recovering PLA nanofibers onto PLA scaffolds produced from 3D-printed filaments [135]. They have proposed two different architectures of the 3D-printed structure, including small amounts of PEG and HA particles to modulate surface and mechanical properties. This allowed for a good compromise in the in vitro cell response regarding biocompatibility and cytoskeleton formation (Figure 5), thus suggesting a promising application for bone regeneration.

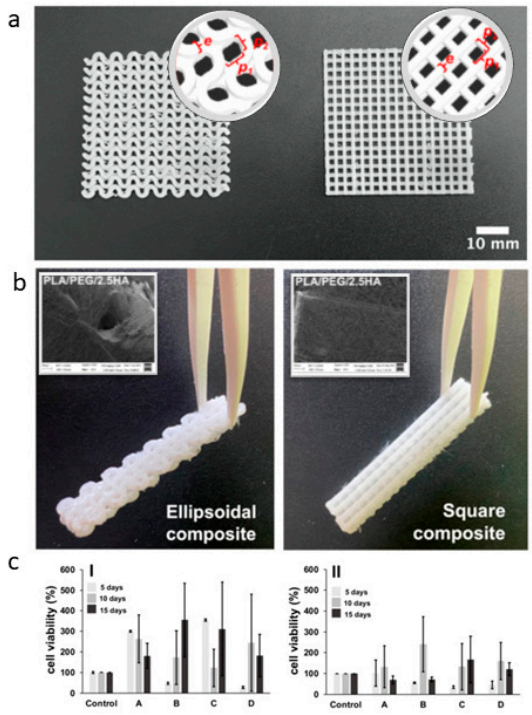



**Figure 5.** PLA-based scaffolds; (**a**) 3D-printed layer macrostructure with ellipsoidal and square pore-shape CAD reconstruction in the round insert); (**b**) 3D-printed/electrospun composite tubes after PLA fibers deposition (electrospun fiber coating in the square); (**c**) In vitro tests via MTT assay of fibroblasts on 3D-printed/electrospun ellipsoidal (**I**) and square (**II**) composites—PLA-based fibers: (A) PLA10, (B) PLA/PEG, (C) PLA/PEG/2.5HA, and (D) PLA/PEG/5.0HA adapted from [135].

In the realm of wound healing, Rezvani Ghomi et al. (2024) designed a porous PCL scaffold printed in a grid pattern and coated it with electrospun PCL/gelatin/ε-polylysine nanofibers. This dual-layer structure exhibited antibacterial properties, suitable mechanical strength, and facilitated fibroblast and keratinocyte alignment, which is critical for skin tissue regeneration [136]. For cardiac applications, Lou et al. (2024) developed myocardial patches with a 3D-printed silicone base to simulate cardiac tissue, onto which aligned and random electrospun PLGA fibers were applied. Their aligned fiber design enhanced mechanical anisotropy, mimicking myocardium properties and demonstrating improved calcium handling in induced pluripotent stem cell-derived cardiomyocytes (hiPSC-CMs), highlighting its potential in cardiac repair [137].

The field of vascular grafts has also benefited from this combination approach, as Fazal et al. (2024) created a gelatin methacryloyl (gelMA) scaffold reinforced with electrospun PCL and PLCL fibers, achieving mechanical compliance like native arteries. This scaffold met the stringent burst pressure and compliance requirements for vascular applications, suggesting its utility for small-diameter arteries [138]. Additionally, Rezaei et al. (2024) developed a dual-layer wound dressing with a 3D-printed PCL layer as support, coated with an electrospun mat of PVA, chitosan, and sildenafil citrate (SC), which accelerated wound closure and collagen deposition in a Wistar rat model [139]. This work collectively underscores how electrospinning onto 3D-printed scaffolds tailors scaffold characteristics for specific TE needs, combining structural integrity with tailored biological responses across cartilage, skin, cardiac, and vascular TE applications.

### *5.2. Three-Dimensional Printing onto Electrospun Fibers*

The approach of "3D printing onto electrospun fibers" merges the structural adaptability of electrospun mats with the mechanical stability of 3D printing. In this approach, scaffolds are first formed by electrospinning nanofibers; these work as a base layer onto which a 3D-printed framework is added, reinforcing the mat and allowing functional layering for specific TE applications.

In the study by Jie Liu et al. (2021), this method is applied to create a hybrid bilayer scaffold for guided bone regeneration. The electrospun layer, made of a heparin-conjugated PCL/gelatin membrane, was a barrier to regulate cell migration, enhancing fibroblast adhesion and cell viability. The 3D-printed layer, composed of PCL/gel/nano-HA, was then deposited onto this electrospun mat to form a supportive structure that enhanced osteogenic activity. Bone marrow stem cells (BMSCs) cultured on this scaffold showed increased osteogenic differentiation with significant BMP-2 expression. In vivo testing in rabbits revealed superior bone regeneration, with significantly higher bone volume to total volume ratios, demonstrating the scaffold's potential for periodontal defect repair [140].

Similarly, Yongteng Song et al. (2024) applied 3D printing to electrospun PCL fibers to construct a bilayer scaffold targeting skin wound repair. Here, the outer electrospun layer contains PCL nanofibers loaded with amoxicillin for antibacterial action, and the 3D-printed inner layer of sodium alginate–gelatin (SG) hydrogel was loaded with recombinant human epidermal growth factor (rhEGF) to promote tissue repair. This bilayer structure displayed antibacterial effects and enhanced cell proliferation, attributed to rhEGF. In a rat model, the scaffold accelerated wound closure and improved collagen deposition, showcasing its capacity for wound healing [141]. Likewise, Cojocaru et al. proposed the fabrication of bicomponent scaffolds by integrating electrospinning and 3D-printing technologies, loaded with a pro-drug/drug coacervate (BiFp@Ht), to serve as an effective platform for wound dressing [142]. In vitro studies demonstrated that both layers could release the loaded therapeutics, exhibiting sustained release profiles (Figure 6).

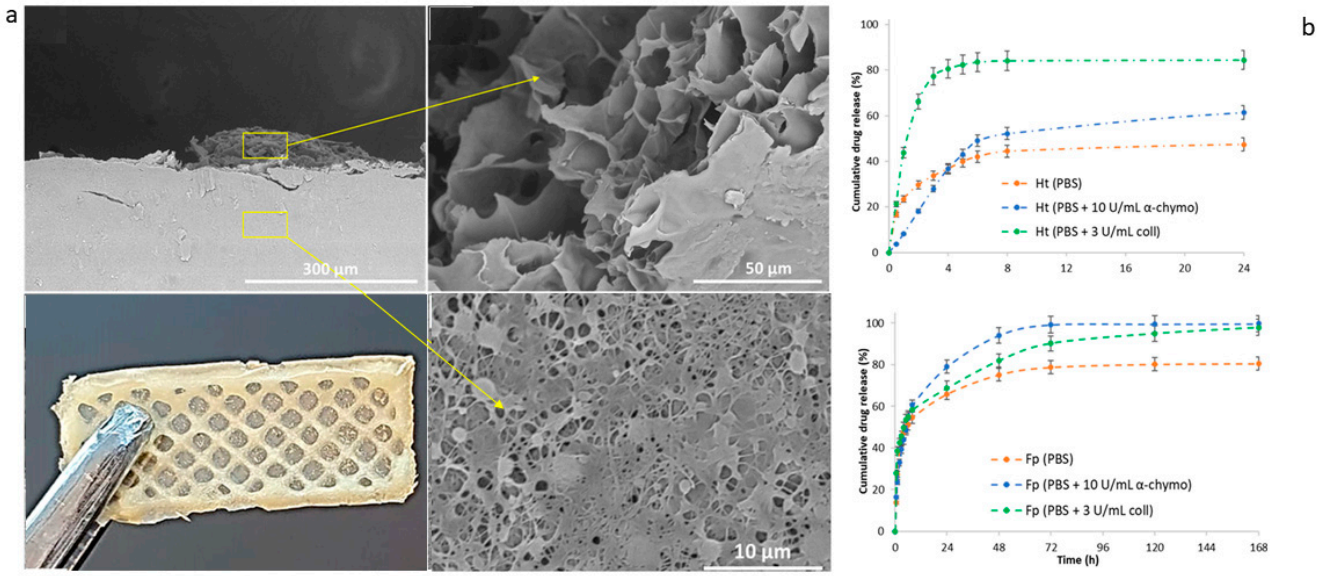



**Figure 6.** Bilayer scaffolds: (**a**) SEM images of lyophilized scaffolds viewed from the cross-section. Yellow arrows highlight specific details of the different regions related to 3D-printed and electrospun membrane compartments. (**b**) Release profiles for the 3D-printed (upper) and electrospun fiber (lower) layers in a PBS solution enriched with degradation agents at varying concentrations. Adapted from [142].

In a distinct application, Nicholas W. Pensa et al. (2019) used the same fabrication method, the 3D printing of a PLA mesh onto an electrospun PCL/gelatin scaffold, to improve the mechanical properties critical for applications in musculoskeletal repair. This PLA reinforcement significantly increased the tensile strength and modulus, up to 1001 ± 302 kPa for the 6 mm mesh, keeping the scaffold's fibrous structure. In vivo, the scaffold demonstrated biocompatibility in rat cranial defects, making it suitable for tissue regeneration requiring enhanced durability, like bone or tendon repair [143]. This combination approach in scaffold fabrication thus achieves dual benefits: the electrospun layer provides a biocompatible, ECM-mimicking surface for cell interactions, and the 3D-printed reinforcement adds structural integrity tailored for various regenerative needs.

### *5.3. Alternate Use of 3D Printing and Electrospinning/Layer-by-Layer*

The alternate use of 3D printing and electrospinning is also known as a sequential layering approach, combining 3D printing and electrospinning. Scaffold fabrication typically begins with the 3D printing of a structural framework that establishes the scaffold's primary shape and mechanical integrity. Then, electrospun fibers are applied in separate layers or sections onto the 3D-printed structure, creating thin, high-surface-area fiber mats that mimic the extracellular matrix and enhance cellular interactions. This process can be repeated to build up layers and produce multilayered, structurally robust scaffolds tailored for specific TE applications, controlled drug release, or antimicrobial properties. The result is a composite scaffold that incorporates the durability and shape fidelity of 3D-printed materials with the biological advantages of nanofiber mats. For example, in small-diameter blood vessel engineering, Atari et al. (2023) demonstrated an effective configuration using helical 3D-printed PCL structures for inner and outer layers combined with electrospun nanofibers made from PCL, PLA, and collagen. The alternating fabrication approach achieved excellent functional integration, resulting in an 80% patency rate in canine femoral arteries, with notable endothelialization and stable blood flow over six months [144]. Similarly, Chen et al. (2023) utilized a trilayered structure for uterine tissue regeneration, where a 4D-printed PLLA-TMC/TPU base layer was enhanced by electro-

spun PLGA/gelatin fibers, followed by a 3D-bioprinted GelMA/gelatin layer with bone marrow stromal cells (BMSCs). The scaffold's shape-morphing ability aligned well with the uterine environment, and the BMSC viability and pH-sensitive estradiol release from the fibers promoted controlled drug delivery, suggesting a robust alternative for uterine repair [145].

For skin tissue regeneration, Mirhaj et al. (2023) fabricated a three-layer scaffold with antibacterial properties by integrating electrospun polyurethane (PU) nanofibers as a microbial barrier, a 3D-printed F127-QCS-AgNO3 middle layer for antibacterial action, and a core–shell electrospun layer loaded with mupirocin for controlled drug release. This multifunctional scaffold displayed high cell viability and antibacterial efficacy, achieving 94% wound closure in rats within 12 days and supporting complete skin regeneration, including hair follicles and glands [146]. Belgheisi et al. (2022) developed a layered construct aimed at bone regeneration, incorporating electrospun PCL nanofibers enriched with pamidronate-layered double hydroxides (PAM-LDH) between two layers of 3D-printed PCL grids. This design delivered a scaffold with structural support and osteogenic potential, demonstrated by enhanced alkaline phosphatase activity, crucial for bone tissue engineering [147].

These studies underscore how the alternate application of 3D printing and electrospinning can yield innovative, application-specific scaffolds that combine durability, functional layering, and tailored release profiles, ultimately enhancing the scaffolds' efficacy in diverse regenerative medicine applications.

### *5.4. Three-Dimensional-Printed Scaffolds Decorated/Infused with Electrospun Nanofibers*

This section explores the innovative approach of "Decorating/Infusing 3D-Printed Scaffolds with Electrospun Nanofiber Segments," which involves embedding electrospun fibers onto pre-formed 3D-printed scaffolds to create composite structures with enhanced mechanical and biological properties. This technique strategically places nanofibers, typically loaded with bioactive agents, on the surface or within specific regions of the scaffold to deliver targeted regenerative benefits while maintaining the structural support provided by the 3D-printed framework. This method allows the integration of the delicate, extracellular matrix-mimicking characteristics of electrospun fibers with the robust, tailored geometry of 3D-printed layers, optimizing scaffold performance across diverse TE applications.

Zhu et al. (2024) explored the application of a bilayer scaffold designed specifically for skull base reconstruction following transnasal surgery. The scaffold combines a radially aligned nanofiber mat of PLCL embedded with basic fibroblast growth factor (bFGF) and a 3D-printed PCL/HA layer. The fabrication technique involved electrospinning the PLCL layer, which was then attached to a softened PCL/HA scaffold through high-temperature treatment, enhancing adhesion and creating a cohesive structure. This bilayer design addresses the dual demands of soft tissue repair and bone regeneration. The electrospun PLCL layer provided a slow release of bFGF, promoting fibroblast proliferation and collagen deposition, essential for dural repair, while the 3D-printed PCL/HA layer with a 300 µm pore size facilitated bone integration. In vivo studies demonstrated promising outcomes, including enhanced bone volume and density in skull defects and improved soft tissue integration, underscoring the scaffold's potential in challenging surgical applications [148]. Similarly, Yilmaz et al. (2024) developed a scaffold for general TE applications by decorating a 3D-printed GelMA hydrogel infused with ciprofloxacin (CIP) for antibacterial properties with electrospun PCL–collagen (COL) fibers, which simulate the extracellular matrix. This method leveraged the moist adhesion of PCL-COL nanofibers to the GelMA scaffold without additional adhesives, creating a bilayer that showed both high cytocompatibility and effective antibacterial action against common pathogens [149].

Each approach illustrates how decorating 3D-printed scaffolds with electrospun nanofibers can tailor scaffold properties to specific applications, from antibacterial surfaces to osteoinductive layers. This showcases the versatility and synergy of these combined fabrication methods in promoting cell viability and targeted tissue regeneration outcomes.

### *5.5. Electrospun Fibers as Inks for 3D Printing*

Using electrospun fibers as bio-inks for 3D printing introduces a powerful method for scaffold fabrication. In this approach, finely structured fibers are repurposed into printable inks that maintain the ECM-like qualities of electrospun fibers while acquiring the structural precision of 3D printing. By processing electrospun fibers into short segments and dispersing them in stabilizing agents, these bio-inks can be extruded through a 3D-printing nozzle, enabling the construction of complex, multifunctional scaffolds that integrate nano- and microscale porosities [150]. This technique represents a sophisticated approach to creating multifunctional scaffolds that fulfill specific therapeutic roles in TE. For instance, He et al. (2024) utilized coaxial electrospinning to produce core–shell nanofibers, combining Protoporphyrin IX (PpIX)/gelatin (GT) for the shell and chondroitin sulfate (CS)/PLGA or HA/PLGA for the core. These nanofibers were then dispersed in a bio-ink composed of polyethylene oxide (PEO) and hyaluronan, allowing the fibers to be directly used in 3D printing. This layered, biphasic scaffold offers "spatiotemporal control," where the upper layer targets anti-tumor activity and the lower layer focuses on osteochondral regeneration. This fabrication process enabled the scaffold to benefit from the fine structure of electrospun fibers, enhancing cell viability, osteogenic differentiation, and in vivo tissue repair in a rabbit model and reducing tumor size in a giant cell tumor of bone (GCTB) mouse model [151].

In a similar vein, Chen et al. (2019) employed electrospun gelatin/PLGA fibers processed into short fragments to serve as inks for 3D printing, which were then combined with hyaluronic acid and PEO to create a stable, printable bio-ink. This method allowed the scaffold to adopt customizable shapes with large, interconnected pores, mimicking the ECM. The resulting structure enhanced mechanical properties and supported high chondrocyte viability, enabling the scaffold to foster cartilage-like tissue formation both in vitro and in vivo. In the rabbit model, the 3DP scaffold demonstrated robust cartilage regeneration and structural durability, maintaining its shape and forming a thicker cartilage layer than control scaffolds. This showcases how transforming electrospun fibers into inks can create ECM-mimicking scaffolds with the versatility and robustness necessary for cartilage tissue engineering [152].

Furthermore, using flexible silica nanofibers as bio-inks within a 3D-printed scaffold introduces an innovative "reinforced concrete" design tailored for bone TE. In Pengfei Cai et al. (2023)'s study, the silica nanofibers were processed into short segments and combined with sodium alginate, creating a bio-ink that supports mechanical stability and biological function. This composite scaffold significantly improved the mechanical properties and increased the elasticity and load-bearing capacity (essential for bone TE), achieving a compressive modulus of 196.0 $\pm$ 22.4 kPa and a compressive stress of 566.6 $\pm$ 128.0 kPa. In vitro, the findings revealed high alkaline phosphatase activity and robust BMSCs' proliferation, indicative of enhanced osteogenic differentiation. In vivo, the scaffold effectively supported new bone formation in a rat cranial defect model, showing superior bone volume and mineral density compared to other scaffold types. Integrating electrospun silica nanofibers into the 3D-printed alginate matrix thus creates a multifunctional scaffold capable of supporting bone growth and repair in complex defect sites [153].

### *5.6. Fabrication of Electrospun Scaffolds on 3D-Printed Collectors/Templates*

Fabricating tailored collectors through 3D printing for electrospinning to guide the deposition of electrospun fibers is an innovative approach to creating scaffolds with precise microarchitectural features and tailored geometries, shapes, fiber alignment, porosity, and mechanical strength. For instance, Zarei et al. (2024) integrated 3D printing with electrospinning to create multilayered tubular structures. They developed a hexagonal pore design in 3D-printed scaffolds, which serve as templates for subsequent electrospinning, achieving a layered structure that effectively mimicked natural vascular constructs. The results showed scaffold-enhanced mechanical properties and significant biocompatibility, as evidenced by in vitro testing with fibroblast cells, suggesting their potential for medical applications in vascular grafting [154].

Similarly, Song et al. (2021) developed a novel method for fabricating TE scaffolds for ear cartilage reconstruction. They performed electrospinning onto a 3D-printed hydrogel collector shaped like ear cartilage. This approach improved nanofibers' uniformity and coverage across complex geometries. The hydrogel, made from a 25:75 blend of alginate and gelatin, was optimized to support this process, ensuring the necessary mechanical properties for the intended application [155]. In a different approach, Holjevac Grgurić et al. (2020) investigated how the geometry of 3D-printed collectors affects the architecture and functionality of PCL scaffolds. Their findings highlighted the significance of collector design, showing that wide-slot, ribbed configurations produced the best cell adhesion and viability results. This study highlights the critical role of scaffold design in tissue regeneration, particularly in environments where antibiotic delivery is crucial [156].

Kasoju et al. (2018) proposed an interesting strategy for cell encapsulation to confine cells and tissues inside a porous reservoir. They have designed a "hollow tank" system starting from a 3D-printed framework containing sodium chloride crystals to be used as a collector for the deposition of electrospun fibers [157]. In the second stage, salts can be removed to form a porous capsule system suitable for cell encapsulation, supporting efficient fluid and molecular transport (Figure 7). Doan et al. (2023) investigated high-resolution fiber deposition using patterned dielectric elastomer collectors, significantly enhancing fiber deposition precision. This method, involving 3D-printed master molds to cast PDMS (polydimethylsiloxane) with conductive materials, underscores the potential of adapting dielectric elastomers to improve the functionality of fiber deposition for applications in biosensors, drug delivery, and TE [158]. Lastly, Brooks-Richards et al. (2022) demonstrated the advantages of using dissolvable PVA molds in melt electrowriting to create tubular scaffolds with complex, patient-specific geometries. This study highlighted that PVA molds were more effective in preserving scaffold morphology and alignment than non-dissolvable PLA molds, emphasizing the non-destructive removal process facilitated by the solubility of PVA. This approach is particularly advantageous for patient-specific TE applications [159].

### *5.7. Platforms Combining 3D-Printing and Electrospinning Techniques*

Platforms that integrate both 3D printing and electrospinning allow these two processes to work in tandem within a single setup, where each layer or section of the scaffold can be alternately printed and electrospun to achieve a cohesive, multi-scale structure. This combination utilizes the precision of 3D printing for structural stability along with the fine fiber networks produced by electrospinning, providing enhanced control over scaffold design in TE applications. In the study by Carranza et al. (2023), the platform setup included a bioprinting unit with a syringe extruder for 3D printing and an electrospinning nozzle that facilitated seamless transitions between the two methods. This alternating process yields a scaffold comprising chitin/gelatin and PVA–gelatin layers, where each layer contributes a distinct scale of porosity, thereby promoting cell adhesion and prolif-

eration. This single-platform design allows the PVA–gelatin nanofibers to be deposited directly onto the 3D-printed gelatin–chitin base, supporting compatibility with human dermal fibroblasts and demonstrating increasing cell viability over time [160]. Similarly, Jiang et al. (2023) reported a setup that integrates far-field jet writing with 3D printing by equipping the platform with electrostatic lenses to control fiber placement precisely. This configuration enables highly organized nanofiber deposition in both 2D and 3D arrangements, achieving a resolution of 200 µm. The system's ability to control fiber positioning makes it particularly useful for biosensing and tissue scaffolding applications that require specific fiber patterns [161].

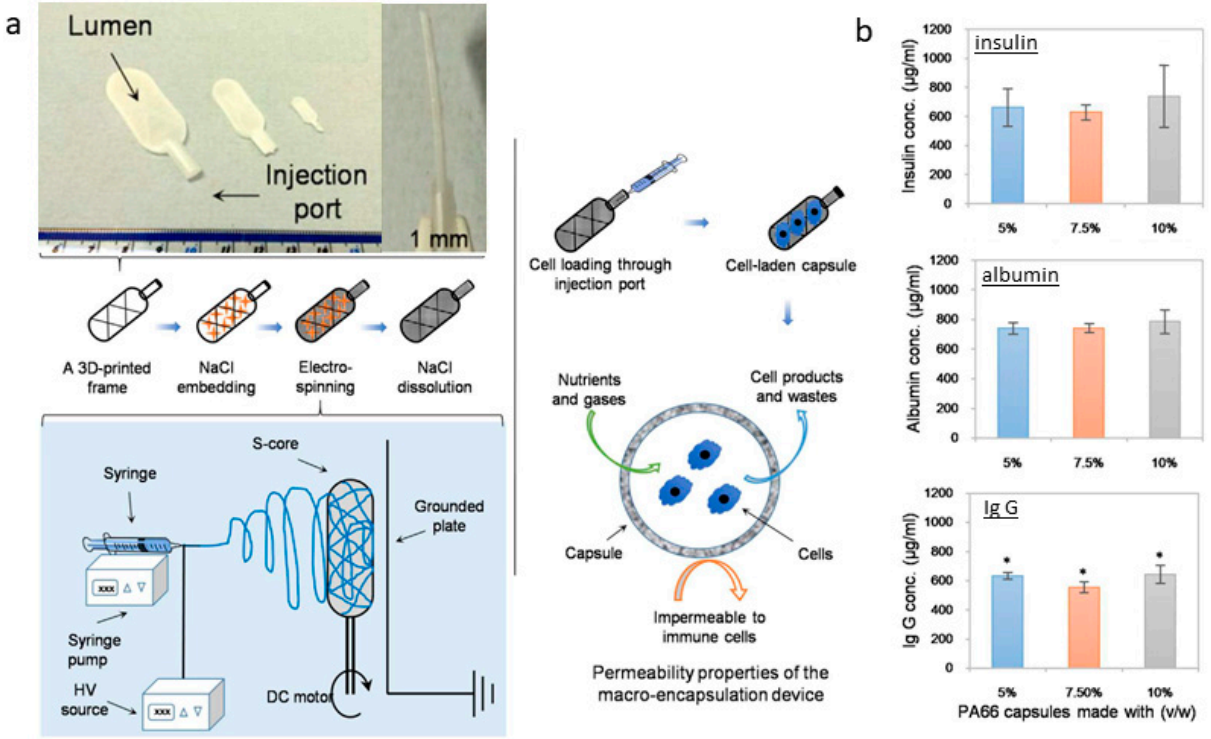



**Figure 7.** Sacrificial core electrospinning capsule: (**a**) Preparation process from the framework production and salt embedding to the deposition of electrospun fibers and the salt-leaching step. The proposed system can load cells, facilitating the free diffusion of nutrients, gases, and cellular waste, as confirmed by protein diffusion assays (**b**). Insulin, albumin, and IgG loaded (1 mg/mL) into the sacrificial core electrospun capsules were shown to diffuse through the membrane into the incubation buffer. Adapted from [157].

Finally, Gonzalez-Pujana et al. (2022) employed a hybrid 3D-printing and electrospinning platform to construct a multi-scale scaffold for bone TE. This setup alternated 3D-printed PCL layers with electrospun PCL nanofiber layers, creating a scaffold that mimics the extracellular matrix (ECM). The platform's integrated design allowed precise layer-by-layer deposition, resulting in a porous structure that promoted bone differentiation. Enhanced ALP activity and increased calcium deposition in vitro demonstrated the scaffold's effectiveness in supporting osteogenic processes, demonstrating its potential in bone TE [162].

Recent findings and applications of this technology's integration in TE are shown and synthesized in Table 3.

**Table 3.** The combination of 3D-printing and electrospinning technologies' applications in TE: fabrication process and findings.

| Approach | Materials and Fabrication Process | Applications | Key Findings | Refs. |
|---|---|---|---|---|
| Electrospinning onto 3D-printed scaffolds | PLA printed scaffold coated with PVA/HLA electrospun fibers | Cartilage TE | Enhanced elastic modulus and tensile strength; increased cell proliferation with chondrocytes. | [133] |
| | PCL printed scaffold layered with BG/Zn and PCL-OST electrospun membrane | Nasal cartilage and bone TE | Improved chondrocyte viability, collagen type II secretion, and cell proliferation. | [134] |
| | 3D-printed PCL grid scaffold with electrospun PCL/gelatin/Îµ-PL nanofibers | Wound healing and skin TE | Enhanced cell alignment, strong antibacterial properties, and skin-like mechanical properties. | [136] |
| | 3D-printed silicone scaffold with aligned PLGA electrospun fibers | Cardiovascular TE | Improved hiPSC-CM alignment, calcium handling, and mechanical anisotropy for myocardium mimicry. | [137] |
| | Extrusion-printed gelMA scaffold reinforced with electrospun PCL/PLCL nanofibers | Cardiovascular TE | High cell viability, compliance suitable for muscular and elastic arteries, high burst pressure. | [138] |
| | 3D-printed PCL membrane with electrospun PVA/CS/SC mat | Wound healing and skin TE | Accelerated wound closure, enhanced collagen deposition, and favorable hydrophilicity. | [139] |
| 3D Printing onto electrospun fibers | 3D printing PCL/Gel/nano-HA onto an electrospun layer of PCL/gelatin | Periodontal defect repair | In vitro: Enhanced fibroblast proliferation on the membrane; BMSCs showed osteogenic differentiation with high BMP-2 expression ($p < 0.001$). In vivo: After 20 weeks, defects treated with a hybrid scaffold had the highest bone volume-to-total volume (BV/TV) ratio ($p < 0.01$). | [140] |
| | 3D printing onto electrospun PCL fibers | Large-scale skin wound repair | In vitro: Antibacterial activity effective against E. coli and S. aureus; HaCaT cells exhibited increased proliferation. In vivo: Higher wound closure rate (89.60 ± 0.83%) in rats by day 14; enhanced collagen deposition and neovascularization. | [141] |
| | 3D printing of a PLA mesh onto an electrospun PCL/gelatin | TE applications requiring enhanced mechanical properties | In vitro: Tensile strength increased to 1001 Â ± 302 kPa with 6 mm PLA mesh reinforcement (13-fold increase). The elastic modulus for a 6 mm mesh was 501 ± 197 kPa ($p < 0.0001$). In vivo: Biocompatibility was confirmed, with no immune response in the rat cranial defect model after 20 weeks. | [143] |
| Alternate use of 3D printing and electrospinning | Alternate 3D printing and electrospinning; PCL helical 3D-printed layers and electrospun PCL/PLA/collagen fibers | Small-diameter blood vessel TE | In vivo: 80% patency rate, endothelialization, ECM deposition, normal blood flow (RI = 0.61, PSV = 39.9 cm/s). | [144] |
| | Alternate 3D printing and electrospinning; PU top layer, 3D-printed F127-QCS-AgNO3 middle, electrospun F127-Mup/Pec-Kr bottom | Skin TE | In vitro: High cell viability, antibacterial, controlled Ag and mupirocin release; In vivo: 94% wound closure rate by day 12. | [146] |
| | Alternate 3D printing and electrospinning; PLLA-TMC/TPU base layer with electrospun PLGA/GT and bioprinted GelMA/GT | Uterine tissue regeneration | In vitro: Shape-morphing, high cell viability, pH-sensitive drug release. | [145] |
| | Alternate 3D printing and electrospinning; PAM-LDH/PCL mats glued between 3D-printed PCL grids | Bone TE | In vitro: Enhanced osteoconductive markers (ALP activity 18.5% increase). | [147] |
| Decorating/Infusing 3D-Printed Scaffolds with Electrospun Nanofiber Segments | Electrospun PLCL embedded with bFGF attached to a 3D-printed PCL/HA layer through high-temperature treatment | Skull base reconstruction | In vitro: Slow bFGF release and enhanced fibroblast proliferation and collagen deposition.In vivo: Enhanced bone volume. | [148] |
| | Decorating 3D-printed GelMA hydrogel infused with ciprofloxacin with electrospun PCL-collagen fibers | TE with antibacterial properties | In vitro: High fibroblast viability (102%) and effective antibacterial properties against *E. coli*, *S. aureus*, and *P. aeruginosa*. Mechanical strength: 24.46 kPa, suitable for biomedical applications. | [149] |

**Table 3.** *Cont.*

| Approach | Materials and Fabrication Process | Applications | Key Findings | Refs. |
|---|---|---|---|---|
| Electrospun fibers as inks for 3D printing | Electrospun fibers were dispersed in a bio-ink composed of polyethylene oxide to produce inks | Osteochondral regeneration and tumor ablation | In vitro: High BMSC viability and enhanced osteogenic and chondrogenic differentiation (e.g., COL1A1 and RUNX2 expression). In vivo: Tumor ablation in GCTB nude mouse model and significant cartilage and bone regeneration in the rabbit model. | [151] |
| | Electrospun GT/PLGA fibers are processed into short fragments to serve as inks for 3D printing | Cartilage regeneration | In vitro: High chondrocyte viability and ECM production in scaffold layers after six weeks. In vivo: Supported cartilage formation and maintained shape post-implantation, forming thicker cartilage than the control in the rabbit model. | [152] |
| | Silica nanofibers were processed into short segments and combined with sodium alginate to create a bio-ink | Bone TE, particularly for cranial bone defect repair | In vitro: Mechanical properties showed compressive stress of 566.6 ± 128.0 kPa and modulus of 196.0 ± 22.4 kPa; high ALP activity and BMSC proliferation with osteogenic marker expression. In vivo: Promoted significant new bone formation in a rat cranial defect model, with the highest bone volume and mineral density among tested scaffolds. | [153] |
| Fabrication of electrospun scaffolds on 3D-printed collectors/templates | Fabrication of multilayered vascular grafts using 3D printing and electrospinning | Vascular grafts for cardiovascular diseases | Successful fabrication demonstrates biocompatibility and mechanical properties suitable for vascular applications. | [154] |
| | Conformal fabrication of nanofibers on 3D ear cartilage-shaped hydrogel collectors | Ear cartilage reconstruction | Enhanced precision in fiber deposition with improved coverage and uniformity on complex shapes. | [155] |
| | Electrospinning of PCL/Cefuroxime on various 3D-printed collector geometries | Tissue regeneration with antibiotic delivery | Wide slot collectors in ribbed configurations enhanced cell adhesion and viability, demonstrating the impact of collector geometry on scaffold performance. | [156] |
| | High-resolution deposition of electrospun fibers on patterned dielectric elastomers | Biosensors, drug delivery systems, and tissue engineering | Patterned dielectric elastomers significantly enhance the precision and control of fiber deposition for medical applications. | [158] |
| | Melt electrowriting on dissolvable PVA molds for tubular scaffolds with patient-specific geometry | TE of vascular and/or anatomically relevant tubular tissues | PVA molds preserved scaffold morphology better than PLA molds, allowing non-destructive removal and maintaining microarchitectural details. | [159] |
| Platforms combining 3D printing electrospinning techniques | Platform setup included a bioprinting unit with a syringe extruder for 3D printing and an electrospinning nozzle | TE, focusing on wound healing | In vitro: Human dermal fibroblasts showed 75% activity at 24 hrs, increasing to 91.8% at 48 hrs and 106.8% at 72 hrs. Cell mortality remained low (~10%). | [160] |
| | Set up that integrates far-field jet writing with 3D printing by equipping the platform with electrostatic lenses | Tissue scaffolding, especially in applications requiring precise fiber arrangement | In vitro: The system achieved 200 µm precision in fiber placement. | [161] |
| | Hybrid 3D-printing and electrospinning platform | Bone TE specifically to induce bone differentiation | In vitro: Significant increase in ALP activity by day 7; calcium deposition up to day 14. Gene expression of ALP and osteopontin markers is upregulated. | [162] |

## 6. Global Patent Landscape for Electrospinning and 3D Printing Scaffolds in TE

In this field, innovation hinges directly on novel applications, methods, and tailored designs for repairing, regenerating, or replacing damaged tissues. The combination of electrospinning, a technique for producing nanofiber networks, and 3D printing, known for its precision in creating tailored geometries, offers significant advantages in developing scaffolds that mimic complex native tissue structures. Patenting these advancements is imperative as each new material, fabrication method, or scaffold design targets specific challenges within TE. Securing intellectual property rights through patents encourages further investment in research and development, ultimately transforming laboratory inno-

vations into practical clinical and commercial applications. This is essential for developing foundational technologies that can shape the future of tissue engineering.

### 6.1. Analysis of Patent Distribution by Geographic Region and Trends over Time

Advances in scaffold fabrication for TE are reflected in the growing number of patents registered worldwide. The numbers continue to increase steadily, and new patents may already have been added to the registry. Among the many platforms available for analyzing patents, the *Espacenet* database stands out as a comprehensive and reliable resource for searching intellectual property worldwide. It allows users to access and review patent registries globally. It offers powerful tools to filter results by keywords, regions, and technological focus, making it one of the most effective resources for exploring the patent landscape in detail.

An extensive search on Espacenet explored the intersection of 3D-printing and electrospinning technologies for nanofibrous scaffold fabrication in TE. The advanced search tool was used to identify patents that explicitly mentioned the keywords "electrospinning," "3D printing," "scaffold," and "tissue engineering" within the same paragraph. This search yielded 140 relevant patents, some of which are analyzed and summarized in Table 4 for further discussion.

**Table 4.** Registered scaffold patents are fabricated by combining 3D-printing and electrospinning technologies and their applications in tissue engineering.

| Patent Title | Summary | Assessments and Findings | Combination Technique | Patent No. |
|---|---|---|---|---|
| Near-Field Direct-Writing Electrospinning 3D Bionic Tendon-Bone Repair Scaffold and Preparation Method | Development of a 3D bionic scaffold for tendon-bone interface repair. Combines 3D printing and near-field direct-writing electrospinning to enhance mechanical properties and biocompatibility. | The final product is a scaffold that can enable stem cells to differentiate to promote tendon and bone repair. In vitro assays showed enhanced cell proliferation. | Alternate use of 3D printing and electrospinning | CN115845136A [163] |
| Composite 3D-Printing Forming System, Forming Method, and Intravascular Stent | Fabrication of vascular stents integrating 3D printing and electrospinning for improved flexibility and strength, suitable for vascular tissue engineering. | The final product is a hollow fibrous stent with branching morphology, mimicking blood vessel structure.The only evaluations presented are visual/photographic fabrication outcomes. | Alternate use of 3D printing and electrospinning | CN106584836A [164] |
| Method of Manufacturing a Medical Device Using 3D Printing and Electrospinning | Fabrication of a multilayered medical device, particularly a scaffold, using a combination of 3D printing and electrospinning | This patent defines a manufacturing method for multilayered medical scaffolds/devices using 3D printing and electrospinning. | Alternate use of 3D printing and electrospinning | WO2023170557A1 [165] |
| A biodegradable meniscus scaffold and its manufacturing method | Development of a scaffold for meniscal cartilage repair using 3D printing and electrospinning. | In vitro, biocompatibility assays demonstrated enhanced cell adhesion and proliferation. | Alternate use of 3D printing and electrospinning | KR20220040773A [166] |
| Multi-Channel Peripheral Nerve Conduit and Preparation Method | Fabrication of a multi-channel nerve conduit for peripheral nerve repair, integrating 3D printing and electrospinning to guide axonal growth and promote regeneration. | Scaffold showed suitable morphology for nerve repair. In vitro assays cells demonstrated cell adhesion and biocompatibility. | Alternate use of 3D printing and electrospinning | CN109172036A [167] |

**Table 4.** *Cont.*

| Patent Title | Summary | Assessments and Findings | Combination Technique | Patent No. |
|---|---|---|---|---|
| Method for Preparing Tendon Scaffold Using 3D-printing and Electrospinning Techniques | Developing a tendon scaffold integrating 3D printing and electrospinning to mimic the natural tendon structure with enhanced mechanical properties and biocompatibility. | Mechanical testing showed suitable tensile strength; in vitro assays demonstrated tendon cell adhesion and proliferation. | Decorating/infusing 3D-printed scaffolds with electrospun nanofiber segments | CN108404213A [168] |
| Method for promoting biological printing myocardial tissue morphological induction by utilizing three-dimensional nanofiber constraint and application of method | Developing a method that enables in situ morphological induction of myocardial tissue during bioprinting by using a 3D aligned nanofiber scaffold that offers topographical cues. | Scaffold promoted cell viability and aligned growth along the fiber orientation. Also, co-printing with endothelial cells enabled the formation of a vascularized engineered myocardial tissue. | 3D-bioprinting onto electrospun fibers. | CN118048298A [169] |
| Method for Preparing Conductive Biological Scaffolds by Melt Jet 3D Printing Driven by Self-Excited Electrostatic Field | A novel hybrid fabrication technique combining melt-jet 3D printing with electrohydrodynamic principles (akin to electrospinning), driven by a self-excited electrostatic field to fabricate a scaffold for TE applications. | High-resolution scaffold structures with controlled porosity and microscale features were achieved | Platforms combining 3D-printing and electrospinning techniques | CN112157906A [170] |
| Systems and methods for optimized patient specific tissue engineering vascular grafts | Fabrication of patient-specific, multi-scale scaffolds by combining 3D printing and electrospinning. The system allows precise placement of nanofiber mats onto anatomical 3D-printed forms, offering great potential for customized biomedical devices | Patient-specific polymeric vascular grafts were created and it was shown that nanofibers can enhance surface area, mimic ECM, or provide bioactivity. | Fabrication of Electrospun Scaffolds on 3D-Printed Collectors/Templates | US11541149B2 [171] |
| Micro-nano composite dual-layer skin ramework and manufacturing method thereof | A composite bilayer scaffold for skin tissue, integrating micro and nanolayers to support skin tissue regeneration with enhanced structural mimicry. | The nanofibrous scaffold provide suitable surface morphology for cell adhesion and growth, thereby facilitating cell adhesion and growth; Scaffold provides a microenvironment for cell growth cells, and facilitates cell infiltration. | Alternate use of 3D printing and electrospinning | CN106110401A [172] |
| Preparation Method Of Multilayer Composite Nano-Micron Fiber Topological Morphology Support With Imitated ECM Structure | Development of a multilayer composite scaffold mimicking ECM structure using 3D printing, electrospinning, or electrostatic spraying, enhancing porosity, fiber diameter control, and tissue support. | SEM and optical images show fiber morphology and layered structures. Fiber diameter (200 nm–3.83 μm), layer thickness (0.4–0.57 mm), pore size (~80 μm), contact angle (114.77°–117.45°) reported. | Alternate use of 3D printing and electrospinning | CN112121232A [173] |

**Table 4.** *Cont.*

| Patent Title | Summary | Assessments and Findings | Combination Technique | Patent No. |
|---|---|---|---|---|
| Artificial blood vessel and the manufacturing method thereof | Artificial blood vessels produced by combining 3D printing and electrospinning in a unified system to combine biocompatibility and mechanical strenght. | An artificial blood vessel was fabricated by combining electrospinning and 3D-printing in a single system. It consists of an inner electrospun microfiber layer, a middle support 3D-printed layer to enhance mechanical strength, and an outer layer of electrospun nanofibers. | Alternate use of 3D printing and electrospinning | KR102467263B1 [174] |
| Preparation of coaxial electrospun-containing multilayered cartilage complex by electrospinning 3D printing | Design of hybrid scaffolds for ligament repair combining 3D printing for structural support with electrospinning for enhanced ligament mimicry and elasticity. | In vitro assays indicated a strong biological effect, shown as an enhanced cell proliferation, and increased collagen production. | Alternate use of 3D printing and electrospinning | CN109701079A [175] |
| Bionic bone tissue engineering scaffold material and preparation method thereof | Multi-layered bone scaffold fabricated via 3D printing, surface biofunctionalization, and bioactive gel infusion with antimicrobial peptides. | Mechanical testing indicated compression strengths comparable to human cortical bone; antibaterial assays showed inhibition rates up to 99%; graudal release of BMP-2 and antimicrobial peptides. | Decorating./infusing 3D-printed scaffolds with electrospun nanofiber segments | CN115054728A [176] |
| Bio-Tubular Scaffold for Fabricating Artificial Vascular and the Fabricating Method Thereof | A method for creating a tubular scaffold for artificial blood vessels thet uses electrospinning for the inner layer and 3D printing for the outer layer to enhance mechanical strength and biocompatibility. | The final product is an scaffold with suitable mechanical strength for vascular applictions. Water uptake, contact angle and chemical characerization are reported. | Decorating/infusing 3D-printed scaffolds with electrospun nanofiber segments | KR101751986B1 [177] |
| Artificial Esophagus Scaffold and Manufacturing Method Thereof | A method for fabricating an artificial esophageal scaffold combining electrospinning and 3D printing to mimic the ECM, providing flexibility and mechanical integrity. | Mechanical testing demonstrated suitable properties for esophageal support; in vitro and in vivo tests showed cell adhesion, with animal studies indicating successful integration. | Alternate use of 3D printing and electrospinning | KR102347096B1 [178] |
| Regeneration bone scaffold forming system and method based on comprehensive 3D printing formation | System and method for fabricating regenerative bone scaffolds using 3D printing, electrospinning, and freeze-drying to enhance porosity and stability for bone regeneration. | This scaffold system enables multi-material integration in a continuous proces to allow patient-specific cutomization and support cell proliferation | Platforms combining 3D-printing and electrospinning techniques | CN103341989A [179] |
| Composite biological 3D printing device and printing method thereof | A method for preparing a biocompatible scaffold for TE made of a 3D-printed PCL base, modified with gelatin nanofibers fabricated by electrospinning. | In vitro assays showed enhanced cell adhesion and good cytocompatibility. | Electrospinning onto 3D bio-printed scaffolds | CN106827496A [180] |

The temporal trend of patent registrations was also analyzed to understand how intellectual property filings in this field have evolved. Notably, there has been a steady and consistent increase in patent filings related to combining these technologies since the

earliest records in 2009. This trend highlights the growing interest in using the combination of electrospinning and 3D printing as a method for manufacturing scaffolds in TE, as illustrated in Figure 8a,b. Two key metrics—earliest priority date and earliest publication date—can be used to track the development of patents in 3D-printing and electrospinning technologies within TE. Both metrics reflect the rising7 interest and progress in this field. Figure 8 shows the annual number of patent families, indicating when inventors filed for intellectual property rights. There has been a consistent increase in patent activity since 2009, with significant peaks in 2015 and 2020, suggesting periods of intensified research and innovation in scaffold fabrication techniques. The red cumulative growth line shows a steady increase over the years, reflecting the ongoing expansion of the field. There has also been a consistent rise in the number of public patents. This coordination between priority and publication dates demonstrates an ongoing interest in the electrospinning and 3D printing of scaffolds, highlighting the need for advanced designs and techniques to meet the demands of tissue regeneration.

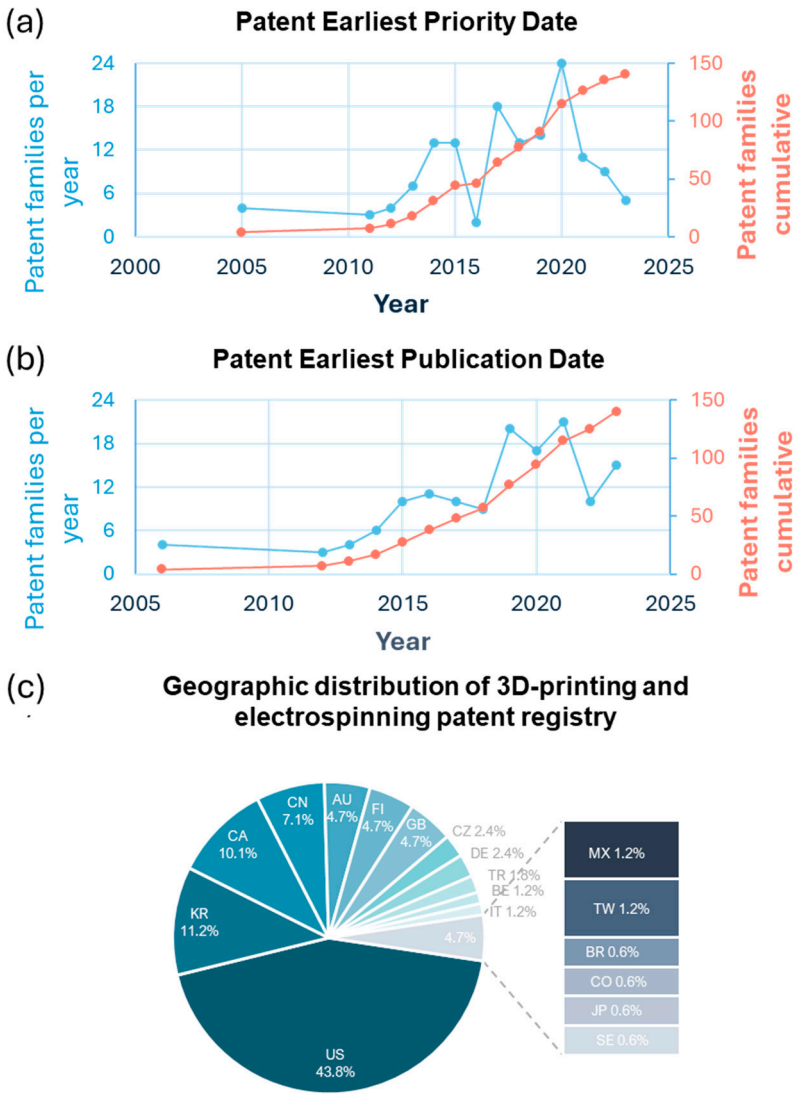



**Figure 8.** Patent trends and geographic distribution in 3D printing and electrospinning. (**a**) Annual and cumulative patent families by earliest priority date. (**b**) Annual and cumulative patent families by earliest publication date. (**c**) Geographic distribution of patent families (%).

Furthermore, Figure 8c illustrates the distribution of registered patents that combine electrospinning and 3D-printing technologies for tissue engineering (TE) applications. The United States leads significantly, accounting for 43.8% of the patent filings, followed by

South Korea at 11.2%, reflecting substantial investment in scaffold technology within Asia. Canada (10.1%) and China (7.1%) are also significant contributors, with additional contributions coming from countries such as Australia, Finland, and the United Kingdom, each representing 4.7% of the total patents. Smaller percentages are observed in countries such as Mexico, Taiwan, and Brazil, each contributing around 1–2%, indicating a growing yet modest contribution from these regions. This international patent distribution reflects widespread interest in these scaffold fabrication methods, with significant research concentrated mainly in North America, Asia, and certain parts of Europe.

### 6.2. Tissue-Specific Applications

The analyzed patents reflect a wide range of tissue-specific applications, each addressing different TEs' unique structural and functional requirements. Many patents focus on bone TE and are designed to replicate the high mechanical bone structure requirements. In cartilage TE, Patent CN106827496A stands out for its approach to creating a scaffold that replicates cartilage's unique, flexible structure. In this work, inventors integrate 3D printing for structural support and electrospinning for surface scaffold enhancement to facilitate chondrocyte adhesion and proliferation, making it well-suited for cartilage repair [180]. For vascular applications, Patent KR101751986B1 presents a bio-tubular scaffold designed to fabricate artificial blood vessels. This scaffold combines an electrospun inner layer, mimicking the ECM, with a 3D-printed outer layer that provides mechanical strength—an ideal structure for supporting vascular tissue [177]. Skin TE is also well-represented, with innovations focused on functional properties such as antibacterial effects. Patent CN115054728A, for example, describes a multi-layered scaffold fabricated via 3D printing, surface biofunctionalization, and bioactive gel infusion with antimicrobial peptides scaffold incorporating antibacterial agents within the electrospun layer to enhance the scaffold's suitability for TE applications by preventing bacterial growth and promoting cell adhesion [176]. Lastly, in nerve TE, Patent CN109172036A describes a multi-channel conduit scaffold for peripheral nerve repair. This scaffold is designed to support axonal growth through multiple pathways, providing a helpful structure to guide nerve regeneration and support cellular growth [167]. An extensive analysis of patent registries is shown in Table 4.

### 6.3. Functional Enhancements

Several patents focus on functional improvements that enhance scaffold performance for various applications. For example, Patent CN115845136A improves scaffold mechanical properties by combining electrospinning with 3D printing. This scaffold shows enhanced tensile strength, making it suitable for high-stress areas, such as tendon–bone junctions [163]. Other patents, such as Patent KR102467263B1, target bioactivity to improve cell attachment and proliferation. This vascular graft scaffold combines 3D-printed and electrospun layers, consisting of an inner electrospun microfiber layer, a middle support 3D-printed layer to enhance mechanical strength, and an outer layer of electrospun nanofibers to create a biocompatible surface that enhances endothelial cell adhesion—essential for vascular applications where bioactivity plays a crucial role in successful integration [174]. Finally, scaffolds with antibacterial properties are particularly notable in skin applications. Patent CN115054728A incorporates antibacterial agents in its electrospun fibers, addressing infection control: an essential feature in tissue regeneration [176].

These patents highlight the versatility of electrospinning and 3D-printing techniques in tailoring scaffolds to meet specific functional requirements. The innovations demonstrated in these patents advance the scaffold's performance in terms of mechanical strength, bioactivity, and antibacterial function and broaden the potential applications of TE in diverse medical fields.

Several patents in this review address key challenges in scaffold fabrication, particularly those related to mechanical instability, biocompatibility, and degradation. Mechanical instability is a significant concern for scaffolds intended for load-bearing applications, such as bone and cartilage. Patents like CN108404213A propose solutions using composite materials and layering electrospun nanofibers over 3D-printed structures to improve tensile and compressive strength, demonstrating suitability for tendon regeneration applications [168]. Biocompatibility is another challenge, as scaffolds must promote cellular adhesion and proliferation without adverse immune responses. As seen in CN115054728A, scaffolds incorporating bioactive components enhance cell attachment, addressing biocompatibility concerns for TE applications. Degradation rates also present a challenge, especially for scaffolds in regenerative medicine. Some patents address this by combining polymers with controlled degradation properties, ensuring the scaffold maintains structural support long enough for tissue regeneration before safely degrading in the body [176,177].

### *6.4. Challenges in Patent Development of TE Scaffolds*

Developing patents that combine 3D printing and electrospinning for TE scaffolds may encounter unique challenges. One primary hurdle is the technical complexity of integrating and combining these two technologies. A precise layering of 3D-printed structures with electrospun nanofibers requires advanced machinery, meticulous control, and attention to detail over variables such as fiber diameter, alignment, and porosity. Also, standardization is a key challenge in this field, as variations in scaffold properties can affect reproducibility and quality, which are crucial for regulatory approval and clinical applications.

### *6.5. Emerging Innovations*

Emerging innovations in TE might shape the future of electrospun and 3D-printed scaffolds. For instance, bioactive scaffolds incorporating bioactive factors or drugs are expected to become more common, enhancing the regenerative potential of complex tissues. Also, innovative scaffolds with controlled drug-release capabilities represent another innovation, offering directed delivery of therapeutic agents supporting healing and preventing infections, particularly in skin and bone applications. Additionally, integrating bioprinting strategies—using living cells in printing processes—could further enhance the ability to create tissue structures that closely mimic natural biology, expanding the potential of scaffold applications in organ regeneration. Indeed, bioprinting methods allow the creation of a 3D spatial arrangement of living cells and biologics into functionalized constructs that mimic the native architecture of natural tissues and organs [181], offering the opportunity to create in vitro/in vivo models to study tissue regeneration and/or tumors and other diseases [182]. The deposition of cells and/or biologics layer by layer can be successfully adapted to using other techniques, such as electrospinning, in different ways. For instance, similar approaches have been used for engineering osteochondral tissues [183] and for the fabrication of biomimetic systems suitable as intervertebral disk equivalents [184] with relevant benefits in terms of biomechanical properties and biological recognition (Figure 9).

Otherwise, the limitations mainly concern high manufacturing costs, system reproducibility, and scalability issues for potential translation into clinical surgery. In this perspective, the use of non-invasive approaches (i.e., in vivo injection of photosensitive cell-laden bio-inks, directly fixed onto the target by near-infrared laser light [185] could be successfully combined with the use of electrospun fibers [186] for the fabrication of fiber-filled bio-inks suitable to efficaciously support molecular diffusion and nutrient supply to cells with significant advantages in terms of cell survival and functionalities (i.e., cell orientation, anisotropic properties), opening new perspectives for a real translation into clinical practice.

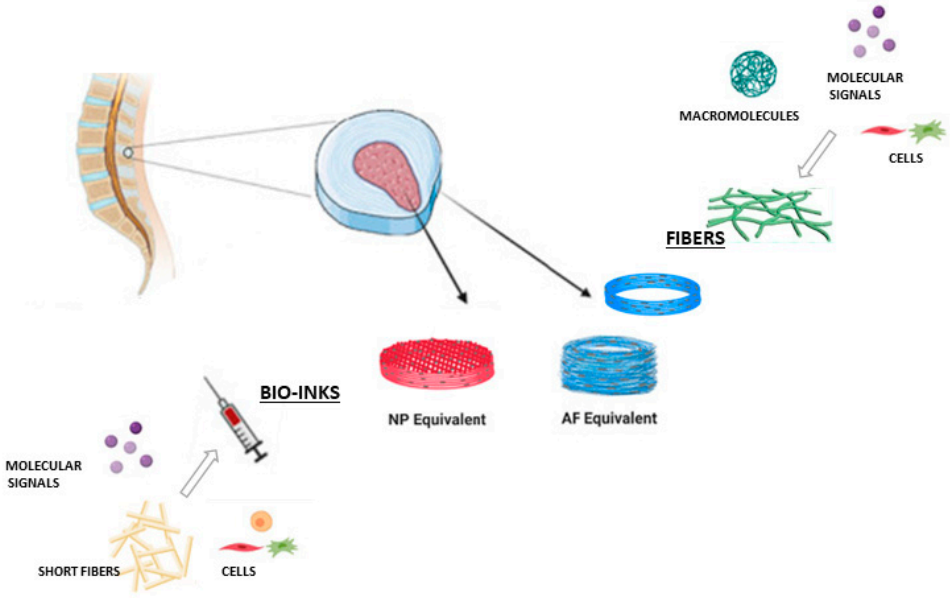



**Figure 9.** Scheme of different strategies for the design of IVD equivalents by integrating bio-inks and electrospun fibers.

## 7. Conclusions

The combination of electrospinning and 3D printing offers a promising alternative for fabricating and manufacturing scaffolds in tissue engineering, as they provide micro- and nanofibrillar membranes that resemble the extracellular matrix and ensure precise geometries on the macro scale and mechanical stability, respectively. This approach to scaffold manufacturing has shown significant advances in TE of bone, skin, nerves, and cardiovascular systems, where improvements in cell adhesion, proliferation, differentiation, and increased mechanical properties for specific demands of different tissues are highlighted. Innovations in this field include multilayered scaffolds, functionalized surfaces, and patient-specific designs. Significant advancements have also been made in controlled drug release and real-time monitoring. The integration of bioprinting further expands applications and future possibilities. Likewise, there is a continuous increase in patent registrations integrating these technologies, highlighting the significant interest in and demand to produce scaffolds with clinical applications in TE. However, there are still challenges that need to be addressed despite the advances that have been made. These challenges include the complexity of integrating these manufacturing methods, the need to standardize, scale, and ensure repeatability, and the additional exploration needed for materials' optimization to ensure cost-effectiveness for broader adoption.

**Author Contributions:** Conceptualization: K.J.J.-N. and M.A.A.-P.; Methodology: K.J.J.-N. and V.G., Formal analysis: K.J.J.-N. and V.G.; Writing—original draft: K.J.J.-N. and M.A.A.-P.; Writing—review and editing: K.J.J.-N., V.G. and M.A.A.-P.; Funding acquisition: M.A.A.-P. and V.G. All authors have read and agreed to the published version of the manuscript.

**Funding:** The present work was funded by a grant from the Universidad Nacional Autónoma de México (UNAM), Dirección General de Asuntos del Personal Académico (DGAPA), Programa de Apoyo a Proyectos de Investigación e Innovación Tecnológica (PAPIIT), DGAPA-UNAM-PAPIIT project number IN202924, and from the European Union—Next-GenerationEU—National Recovery and Resilience Plan (NRRP)—MISSION 4 COMPONENT 2, INVESTMENT N. 1.1, CALL PRIN 2022 PNRR D.D. 1409 14-09-2022—Project Title: Role of extracellular matrix in controlling macrophage cell response to nanomaterials (TRAMA) (n. P2022LPTSF).

**Data Availability Statement:** All relevant data are within the paper.

**Acknowledgments:** Karen J. Juarez-Navarro appreciates the support of the Secretaria de Ciencia, Humanidades, Tecnología e Innovación (SECIHTI), through its doctoral scholarship (CVU: 992640) for her PhD studies in the Posgrado en Ciencias Biológicas, Facultad de Ciencias, UNAM. The authors also thank MSc. C.E. Torres-Salcido for his technical support in providing the SEM micrographs used in Figure 2.

**Conflicts of Interest:** The authors declare that they have no known competing financial interests or personal relationships that could have influenced the work reported in this study. All authors have read and accepted the published version of this manuscript.

## References

1. Moysidou, C.M.; Barberio, C.; Owens, R.M. Advances in Engineering Human Tissue Models. *Front. Bioeng. Biotechnol.* **2021**, *8*, 620962. [CrossRef] [PubMed]
2. Adel, I.M.; Elmeligy, M.F.; Elkasabgy, N.A. Conventional and Recent Trends of Scaffolds Fabrication: A Superior Mode for Tissue Engineering. *Pharmaceutics* **2022**, *14*, 306. [CrossRef]
3. Ferraris, S.; Spriano, S.; Scalia, A.C.; Cochis, A.; Rimondini, L.; Cruz-Maya, I.; Guarino, V.; Varesano, A.; Vineis, C. Topographical and Biomechanical Guidance of Electrospun Fibers for Biomedical Applications. *Polymers* **2020**, *12*, 2896. [CrossRef] [PubMed]
4. Suamte, L.; Tirkey, A.; Barman, J.; Jayasekhar Babu, P. Various Manufacturing Methods and Ideal Properties of Scaffolds for Tissue Engineering Applications. *Smart Mater. Manuf.* **2023**, *1*, 100011. [CrossRef]
5. Saracino, E.; Cirillo, V.; Marrese, M.; Guarino, V.; Benfenati, V.; Zamboni, R.; Ambrosio, L. Structural and Functional Properties of Astrocytes on PCL Based Electrospun Fibres. *Mater. Sci. Eng. C* **2021**, *118*, 111363. [CrossRef]
6. Zulkifli, M.Z.A.; Nordin, D.; Shaari, N.; Kamarudin, S.K. Overview of Electrospinning for Tissue Engineering Applications. *Polymers* **2023**, *15*, 2418. [CrossRef]
7. Guarino, V.; Cruz-Maya, I.; Altobelli, R.; Abdul Khodir, W.K.; Ambrosio, L.; Alvarez Pèrez, M.A.; Flores, A.A. Electrospun Polycaprolactone Nanofibres Decorated by Drug Loaded Chitosan Nano-Reservoirs for Antibacterial Treatments. *Nanotechnology* **2017**, *28*, 505103. [CrossRef]
8. Mu, J.; Luo, D.; Li, W.; Ding, Y. Multiscale Polymeric Fibers for Drug Delivery and Tissue Engineering. *Biomed. Technol.* **2024**, *5*, 60–72. [CrossRef]
9. Ghosh, A.; Orasugh, J.T.; Ray, S.S.; Chattopadhyay, D. Integration of 3D Printing-Coelectrospinning: Concept Shifting in Biomedical Applications. *ACS Omega* **2023**, *8*, 28002–28025. [CrossRef]
10. Yang, D.L.; Faraz, F.; Wang, J.X.; Radacsi, N. Combination of 3D Printing and Electrospinning Techniques for Biofabrication. *Adv. Mater. Technol.* **2022**, *7*, 2101309. [CrossRef]
11. Ramakrishna, S. *An Introduction to Electrospinning and Nanofibers*; World Scientific Publishing: Singapore, 2005.
12. Neves, N.M. *Electrospinning for Advanced Biomedical Applications and Therapies*; Smithers Rapra Technology, Ltd.: Shropshire, UK, 2012; ISBN 9781847356000.
13. Chinnappan, B.A.; Krishnaswamy, M.; Xu, H.; Hoque, M.E. Electrospinning of Biomedical Nanofibers/Nanomembranes: Effects of Process Parameters. *Polymers* **2022**, *14*, 3719. [CrossRef] [PubMed]
14. Alharbi, N.; Daraei, A.; Lee, H.; Guthold, M. The Effect of Molecular Weight and Fiber Diameter on the Mechanical Properties of Single, Electrospun PCL Nanofibers. *Mater. Today Commun.* **2023**, *35*, 105773. [CrossRef]
15. Yalcinkaya, F.; Jirsak, O.; Gemci, R. Effect of Polymer Concentration on Electrospinning System. In Proceedings of the Fiber Society Spring 2010 International Conference, Bursa, Turkey, 12–14 May 2010.
16. Liu, Z.; Ramakrishna, S.; Ahmed, I.; Rudd, C.; Liu, X. Rheological, Surface Tension and Conductivity Insights on the Electrospinnability of Poly(Lactic-Co-Glycolic Acid)-Hyaluronic Acid Solutions and Their Correlations with the Nanofiber Morphological Characteristics. *Polymers* **2022**, *14*, 4411. [CrossRef]
17. Higashi, S.; Hirai, T.; Matsubara, M.; Yoshida, H.; Beniya, A. Dynamic Viscosity Recovery of Electrospinning Solution for Stabilizing Elongated Ultrafine Polymer Nanofiber by TEMPO-CNF. *Sci. Rep.* **2020**, *10*, 13427. [CrossRef]
18. Asran, A.S.; Salama, M.; Popescu, C.; Michler, G.H. Solvent Influences the Morphology and Mechanical Properties of Electrospun Poly(L-Lactic Acid) Scaffold for Tissue Engineering Applications. *Macromol. Symp.* **2010**, *294*, 153–161. [CrossRef]
19. Luo, C.J.; Nangrejo, M.; Edirisinghe, M. A Novel Method of Selecting Solvents for Polymer Electrospinning. *Polymer* **2010**, *51*, 1654–1662. [CrossRef]
20. Uyar, T.; Besenbacher, F. Electrospinning of Uniform Polystyrene Fibers: The Effect of Solvent Conductivity. *Polymer* **2008**, *49*, 5336–5343. [CrossRef]
21. Abdulhussain, R.; Adebisi, A.; Conway, B.R.; Asare-Addo, K. Electrospun Nanofibers: Exploring Process Parameters, Polymer Selection, and Recent Applications in Pharmaceuticals and Drug Delivery. *J. Drug Deliv. Sci. Technol.* **2023**, *90*, 105156. [CrossRef]

22. Samatham, R.; Kim, K.J. Electric Current as a Control Variable in the Electrospinning Process. *Polym. Eng. Sci.* **2006**, *46*, 954–959. [CrossRef]
23. Elveren, B.; Kurečič, M.; Maver, T.; Maver, U. Cell Electrospinning: A Mini-Review of the Critical Processing Parameters and Its Use in Biomedical Applications. *Adv. Biol.* **2023**, *7*, 2300057. [CrossRef]
24. Matabola, K.P.; Moutloali, R.M. The Influence of Electrospinning Parameters on the Morphology and Diameter of Poly(Vinyledene Fluoride) Nanofibers—Effect of Sodium Chloride. *J. Mater. Sci.* **2013**, *48*, 5475–5482. [CrossRef]
25. Utkarsh; Hegab, H.; Tariq, M.; Syed, N.A.; Rizvi, G.; Pop-Iliev, R. Towards Analysis and Optimization of Electrospun PVP (Polyvinylpyrrolidone) Nanofibers. *Adv. Polym. Technol.* **2020**, *2020*, 4090747. [CrossRef]
26. Syed Bakar, S.S.; Foong, K.M.; Abdul Halif, N.; Yahud, S. Effect of Solution Concentration and Applied Voltage on Electrospun Polyacrylonitrile Fibers. In *Proceedings of the IOP Conference Series: Materials Science and Engineering*; IOP Publishing Ltd.: Bristol, UK, 2019; Volume 701.
27. Liu, Z.; Ju, K.; Wang, Z.; Li, W.; Ke, H.; He, J. Electrospun Jets Number and Nanofiber Morphology Effected by Voltage Value: Numerical Simulation and Experimental Verification. *Nanoscale Res. Lett.* **2019**, *14*, 310. [CrossRef]
28. Jacobs, V.; Anandjiwala, R.D.; Maaza, M. The Influence of Electrospinning Parameters on the Structural Morphology and Diameter of Electrospun Nanofibers. *J. Appl. Polym. Sci.* **2010**, *115*, 3130–3136. [CrossRef]
29. Hasanzadeh, M.; Moghadam, B.H.; Abatari, M.H.M.; Haghi, A.K. On the Production Optimization of Polyacrylonitrile Electrospun Nanofiber. *Bulg. Chem. Commun.* **2013**, *45*, 178–190.
30. Duan, Y.; Kalluri, L.; Satpathy, M.; Duan, Y. Effect of Electrospinning Parameters on the Fiber Diameter and Morphology of PLGA Nanofibers. *Dent. Oral. Biol. Craniofacial Res.* **2021**, *2021*, 1–7. [CrossRef]
31. Ranjbar-Mohammadi, M.; Bahrami, S.H.; Joghataei, M.T. Fabrication of Novel Nanofiber Scaffolds from Gum Tragacanth/Poly(Vinyl Alcohol) for Wound Dressing Application: In Vitro Evaluation and Antibacterial Properties. *Mater. Sci. Eng. C* **2013**, *33*, 4935–4943. [CrossRef]
32. Herrero-Herrero, M.; Gómez-Tejedor, J.A.; Vallés-Lluch, A. PLA/PCL Electrospun Membranes of Tailored Fibres Diameter as Drug Delivery Systems. *Eur. Polym. J.* **2018**, *99*, 445–455. [CrossRef]
33. He, H.; Kara, Y.; Molnar, K. Effect of Needle Characteristic on Fibrous PEO Produced by Electrospinning. *Resolut. Discov.* **2019**, *4*, 7–11. [CrossRef]
34. Barua, B.; Saha, M.C. Influence of Humidity, Temperature, and Annealing on Microstructure and Tensile Properties of Electrospun Polyacrylonitrile Nanofibers. *Polym. Eng. Sci.* **2018**, *58*, 998–1009. [CrossRef]
35. Raksa, A.; Numpaisal, P.O.; Ruksakulpiwat, Y. The Effect of Humidity during Electrospinning on Morphology and Mechanical Properties of SF/PVA Nanofibers. *Mater. Today Proc.* **2021**, *47*, 3458–3461. [CrossRef]
36. Park, B.K.; Um, I.C. Effect of Relative Humidity on the Electrospinning Performance of Regenerated Silk Solution. *Polymers* **2021**, *13*, 2479. [CrossRef]
37. Rashid, T.U.; Gorga, R.E.; Krause, W.E. Mechanical Properties of Electrospun Fibers—A Critical Review. *Adv. Eng. Mater.* **2021**, *23*, 2100153. [CrossRef]
38. Langer, R.; Vacanti, J. Advances in Tissue Engineering. *J. Pediatr. Surg.* **2016**, *51*, 8–12. [CrossRef] [PubMed]
39. Ikada, Y. Challenges in Tissue Engineering. *J. R. Soc. Interface* **2006**, *3*, 589–601. [CrossRef]
40. Flores-Rojas, G.G.; Gómez-Lazaro, B.; López-Saucedo, F.; Vera-Graziano, R.; Bucio, E.; Mendizábal, E. Electrospun Scaffolds for Tissue Engineering: A Review. *Macromol* **2023**, *3*, 524–553. [CrossRef]
41. Rahmati, M.; Mills, D.K.; Urbanska, A.M.; Saeb, M.R.; Venugopal, J.R.; Ramakrishna, S.; Mozafari, M. Electrospinning for Tissue Engineering Applications. *Prog. Mater. Sci.* **2021**, *117*, 100721. [CrossRef]
42. Guarino, V.; Ambrosio, L. Electrofluidodynamics: Exploring a New Toolbox to Design Biomaterials for Tissue Regeneration and Degeneration. *Nanomedicine* **2016**, *11*, 1515–1518. [CrossRef]
43. Meng, C.; Liu, X.; Li, R.; Malekmohammadi, S.; Feng, Y.; Song, J.; Gong, R.H.; Li, J. 3D Poly (L-Lactic Acid) Fibrous Sponge with Interconnected Porous Structure for Bone Tissue Scaffold. *Int. J. Biol. Macromol.* **2024**, *268*, 131688. [CrossRef]
44. Kalidas, S.; Sumathi, S. Copper Substituted Hydroxyapatite Reinforced Gelatin/Polyvinyl Alcohol/Silk Fibre-Based Scaffold for Bone Tissue Engineering Application. *Mater. Chem. Phys.* **2024**, *320*, 129410. [CrossRef]
45. García, G.; Moreno-Serna, V.; Saavedra, M.; Cordoba, A.; Canales, D.; Alfaro, A.; Guzmán-Soria, A.; Orihuela, P.; Zapata, S.; Grande-Tovar, C.D.; et al. Electrospun Scaffolds Based on a PCL/Starch Blend Reinforced with CaO Nanoparticles for Bone Tissue Engineering. *Int. J. Biol. Macromol.* **2024**, *273*, 132891. [CrossRef]
46. Canales, D.A.; Reyes, F.; Saavedra, M.; Peponi, L.; Leonés, A.; Palza, H.; Boccaccini, A.R.; Grünewald, A.; Zapata, P.A. Electrospun Fibers of Poly (Lactic Acid) Containing Bioactive Glass and Magnesium Oxide Nanoparticles for Bone Tissue Regeneration. *Int. J. Biol. Macromol.* **2022**, *210*, 324–336. [CrossRef] [PubMed]
47. Eren Boncu, T.; Uskudar Guclu, A.; Catma, M.F.; Savaser, A.; Gokce, A.; Ozdemir, N. In Vitro and in Vivo Evaluation of Linezolid Loaded Electrospun PLGA and PLGA/PCL Fiber Mats for Prophylaxis and Treatment of MRSA Induced Prosthetic Infections. *Int. J. Pharm.* **2020**, *573*, 118758. [CrossRef] [PubMed]

48. Sun, D.; Sun, X.; Li, D.; Wang, M.; Song, S.; Liu, C.; Ma, N.; Yin, X.; Wang, C. UCNPs-Labeled Electrospun Scaffolds Used to Monitor in Vivo Degradation and Bone Tissue Regeneration. *Colloids Surf. B Biointerfaces* **2024**, *237*, 113860. [CrossRef] [PubMed]
49. Anjum, S.; Li, T.; Arya, D.K.; Ali, D.; Alarifi, S.; Yulin, W.; Hengtong, Z.; Rajinikanth, P.S.; Ao, Q. Biomimetic Electrospun Nanofibrous Scaffold for Tissue Engineering: Preparation, Optimization by Design of Experiments (DOE), in-Vitro and in-Vivo Characterization. *Front. Bioeng. Biotechnol.* **2023**, *11*, 1288539. [CrossRef] [PubMed]
50. Shadman-Manesh, V.; Gholipour-Kanani, A.; Najmoddin, N.; Rabbani, S. Preclinical Evaluation of the Polycaprolactone-Polyethylene Glycol Electrospun Nanofibers Containing Egg-Yolk Oil for Acceleration of Full Thickness Burns Healing. *Sci. Rep.* **2023**, *13*, 919. [CrossRef]
51. Lizarazo-Fonseca, L.; Correa-Araujo, L.; Prieto-Abello, L.; Camacho-Rodríguez, B.; Silva-Cote, I. In Vitro and in Vivo Evaluation of Electrospun Poly (ε-Caprolactone)/Collagen Scaffolds and Wharton's Jelly Mesenchymal Stromal Cells (HWJ-MSCs) Constructs as Potential Alternative for Skin Tissue Engineering. *Regen. Ther.* **2023**, *24*, 11–24. [CrossRef]
52. Sanchez Ramirez, D.O.; Cruz-Maya, I.; Vineis, C.; Tonetti, C.; Varesano, A.; Guarino, V. Design of Asymmetric Nanofibers-Membranes Based on Polyvinyl Alcohol and Wool-Keratin for Wound Healing Applications. *J. Funct. Biomater.* **2021**, *12*, 76. [CrossRef]
53. Shahghasempour, L.; Fattahi, R.; Hosseinzadeh, S.; Haddadi, A.; Shams, F. In Vivo Assessment of Lactobacillus Plantarum and Co-Cultured Cells on a Polyurethane/PRGF/Gelatin/Polyurethane Scaffold in Skin Wound Healing. *SPE Polym.* **2024**, *5*, 637–662. [CrossRef]
54. Du, P.; Chen, X.; Chen, Y.; Li, J.; Lu, Y.; Li, X.; Hu, K.; Chen, J.; Lv, G. In Vivo and in Vitro Studies of a Propolis-Enriched Silk Fibroin-Gelatin Composite Nanofiber Wound Dressing. *Heliyon* **2023**, *9*, e13506. [CrossRef]
55. Petrova, V.A.; Poshina, D.N.; Golovkin, A.S.; Mishanin, A.I.; Zhuravskii, S.G.; Yukina, G.Y.; Naumenko, M.Y.; Sukhorukova, E.G.; Savin, N.A.; Erofeev, A.S.; et al. Electrospun Composites of Chitosan with Cerium Oxide Nanoparticles for Wound Healing Applications: Characterization and Biocompatibility Evaluation In Vitro and In Vivo. *Polymers* **2024**, *16*, 1787. [CrossRef] [PubMed]
56. Ali, I.H.; Khalil, I.A.; El-Sherbiny, I.M. Design, Development, in-Vitro and in-Vivo Evaluation of Polylactic Acid-Based Multifunctional Nanofibrous Patches for Efficient Healing of Diabetic Wounds. *Sci. Rep.* **2023**, *13*, 3215. [CrossRef] [PubMed]
57. Husain, K.; Malik, A.; Kirchens, J.; Choi, G. A Prospective, Blinded, Randomized Controlled Clinical Trial Evaluating the Effect of the Synthetic Electrospun Fiber Matrix in the Treatment of Chronic Diabetic Foot Ulcers. *Foot Ankle Surg. Tech. Rep. Cases* **2024**, *4*, 100362. [CrossRef]
58. Carrabba, M.; Fagnano, M.; Ghorbel, M.T.; Rapetto, F.; Su, B.; De Maria, C.; Vozzi, G.; Biglino, G.; Perriman, A.W.; Caputo, M.; et al. Development of a Novel Hierarchically Biofabricated Blood Vessel Mimic Decorated with Three Vascular Cell Populations for the Reconstruction of Small-Diameter Arteries. *Adv. Funct. Mater.* **2024**, *34*, 2300621. [CrossRef] [PubMed]
59. Xiao, Y.; Cai, Z.; Xing, Y.; Fang, Z.; Ye, L.; Geng, X.; Zhang, A.-Y.; Gu, Y.; Feng, Z.-G. Fabrication of Small-Diameter in Situ Tissue Engineered Vascular Grafts with Core/Shell Fibrous Structure and a One-Year Evaluation via Rat Abdominal Vessel Replacement Model. *Biomater. Adv.* **2024**, *165*, 214018. [CrossRef]
60. Wei, X.; Wang, L.; Duan, C.; Chen, K.; Li, X.; Guo, X.; Chen, P.; Liu, H.; Fan, Y. Cardiac Patches Made of Brown Adipose-Derived Stem Cell Sheets and Conductive Electrospun Nanofibers Restore Infarcted Heart for Ischemic Myocardial Infarction. *Bioact. Mater.* **2023**, *27*, 271–287. [CrossRef]
61. Liu, Y.; Wang, L.; Liu, Z.; Kang, Y.; Chen, T.; Xu, C.; Zhu, T. Durable Immunomodulatory Nanofiber Niche for the Functional Remodeling of Cardiovascular Tissue. *ACS Nano* **2024**, *18*, 951–971. [CrossRef]
62. Handley, E.L.; Callanan, A. Effects of Electrospun Fibers Containing Ascorbic Acid on Oxidative Stress Reduction for Cardiac Tissue Engineering. *J. Appl. Polym. Sci.* **2023**, *140*, e54242. [CrossRef]
63. Liu, S.; Yao, L.; Wang, Y.; Li, Y.; Jia, Y.; Yang, Y.; Li, N.; Hu, Y.; Kong, D.; Dong, X.; et al. Immunomodulatory Hybrid Micro-Nanofiber Scaffolds Enhance Vascular Regeneration. *Bioact. Mater.* **2023**, *21*, 464–482. [CrossRef]
64. Chernonosova, V.S.; Osipova, O.; Nuankai, Z.; Shundrina, I.; Murashov, I.S.; Larichev, Y.; Karpenko, A.A.; Laktionov, P.P. Evaluation of Properties for Carbothane™ 3575A–Based Electrospun Vascular Grafts in Vitro and in Vivo. *Biomed. Mater.* **2024**, *19*, 065012. [CrossRef]
65. Xie, B.; Ma, H.; Yang, F.; Chen, H.; Guo, Y.; Zhang, H.; Li, T.; Huang, X.; Zhao, Y.; Li, X.; et al. Development and Evaluation of 3D Composite Scaffolds with Piezoelectricity and Biofactor Synergy for Enhanced Articular Cartilage Regeneration. *J. Mater. Chem. B* **2024**, *12*, 10416–10433. [CrossRef] [PubMed]
66. Zhang, Y.; Cai, R.; Li, J.; Wu, X. The Immunosuppressive Niche Established with a Curcumin-Loaded Electrospun Nanofibrous Membrane Promotes Cartilage Regeneration in Immunocompetent Animals. *Membranes* **2023**, *13*, 335. [CrossRef]
67. Huo, Y.; Bai, B.; Zheng, R.; Sun, Y.; Yu, Y.; Wang, X.; Chen, H.; Hua, Y.; Zhang, Y.; Zhou, G.; et al. In Vivo Stable Allogenic Cartilage Regeneration in a Goat Model Based on Immunoisolation Strategy Using Electrospun Semipermeable Membranes. *Adv. Healthc. Mater.* **2023**, *12*, e2203084. [CrossRef]

68. Fasolino, I.; Guarino, V.; Cirillo, V.; Ambrosio, L. 5-Azacytidine-Mediated HMSC Behavior on Electrospun Scaffolds for Skeletal Muscle Regeneration. *J. Biomed. Mater. Res. A* **2017**, *105*, 2551–2561. [CrossRef]
69. Abdulmalik, S.; Gallo, J.; Nip, J.; Katebifar, S.; Arul, M.; Lebaschi, A.; Munch, L.N.; Bartly, J.M.; Choudhary, S.; Kalajzic, I.; et al. Nanofiber Matrix Formulations for the Delivery of Exendin-4 for Tendon Regeneration: In Vitro and in Vivo Assessment. *Bioact. Mater.* **2023**, *25*, 42–60. [CrossRef] [PubMed]
70. Iorio, F.; El Khatib, M.; Wöltinger, N.; Turriani, M.; Di Giacinto, O.; Mauro, A.; Russo, V.; Barboni, B.; Boccaccini, A.R. Electrospun Poly(ε-Caprolactone)/Poly(Glycerol Sebacate) Aligned Fibers Fabricated with Benign Solvents for Tendon Tissue Engineering. *J. Biomed. Mater. Res. A* **2025**, *113*, e37794. [CrossRef] [PubMed]
71. Liu, J.; Chen, L.; Sun, Z.; Tao, Z.; Pavel, V.; Li, Y.; Wang, F.; Cui, W.; Liu, S. Unidirectional Gene Delivery Electrospun Fibrous Membrane via Charge Repulsion for Tendon Repair. *Bioact. Mater.* **2024**, *37*, 191–205. [CrossRef]
72. Xiong, F.; Wei, S.; Wu, S.; Jiang, W.; Li, B.; Xuan, H.; Xue, Y.; Yuan, H. Aligned Electroactive Electrospun Fibrous Scaffolds for Peripheral Nerve Regeneration. *ACS Appl. Mater. Interfaces* **2023**, *15*, 41385–41402. [CrossRef]
73. Wei, S.; Xiong, F.; Gu, H.; Zhang, Z.; Xuan, H.; Jin, Y.; Xue, Y.; Li, B.; Feng, W.; Yuan, H. Highly Aligned Electroactive Ultrafine Fibers Promote the Differentiation of Mesenchymal Stem Cells into Schwann-like Cells for Nerve Regeneration. *Int. J. Biol. Macromol.* **2024**, *279*, 135388. [CrossRef]
74. Ma, Y.; Zhang, R.; Mao, X.; Li, X.; Li, T.; Liang, F.; He, J.; Wen, L.; Wang, W.; Li, X.; et al. Preparation of PLCL/ECM Nerve Conduits by Electrostatic Spinning Technique and Evaluation in Vitro and in Vivo. *J. Neural Eng.* **2024**, *21*, 026028. [CrossRef]
75. Puhl, D.L.; Funnell, J.L.; Fink, T.D.; Swaminathan, A.; Oudega, M.; Zha, R.H.; Gilbert, R.J. Electrospun Fiber-Mediated Delivery of Neurotrophin-3 MRNA for Neural Tissue Engineering Applications. *Acta Biomater.* **2023**, *155*, 370–385. [CrossRef] [PubMed]
76. Pires, L.R.; Guarino, V.; Oliveira, M.J.; Ribeiro, C.C.; Barbosa, M.A.; Ambrosio, L.; Pêgo, A.P. Ibuprofen-Loaded Poly(Trimethylene Carbonate-Co-ε-Caprolactone) Electrospun Fibres for Nerve Regeneration. *J. Tissue Eng. Regen. Med.* **2016**, *10*, E154–E166. [CrossRef] [PubMed]
77. Mao, X.; Li, T.; Cheng, J.; Tao, M.; Li, Z.; Ma, Y.; Javed, R.; Bao, J.; Liang, F.; Guo, W.; et al. Nerve ECM and PLA-PCL Based Electrospun Bilayer Nerve Conduit for Nerve Regeneration. *Front. Bioeng. Biotechnol.* **2023**, *11*, 1103435. [CrossRef]
78. Gautam, S.; Sharma, C.; Purohit, S.D.; Singh, H.; Dinda, A.K.; Potdar, P.D.; Chou, C.F.; Mishra, N.C. Gelatin-Polycaprolactone-Nanohydroxyapatite Electrospun Nanocomposite Scaffold for Bone Tissue Engineering. *Mater. Sci. Eng. C* **2021**, *119*, 111588. [CrossRef] [PubMed]
79. Movahedi, M.; Asefnejad, A.; Rafienia, M.; Khorasani, M.T. Potential of Novel Electrospun Core-Shell Structured Polyurethane/Starch (Hyaluronic Acid) Nanofibers for Skin Tissue Engineering: In Vitro and in Vivo Evaluation. *Int. J. Biol. Macromol.* **2020**, *146*, 627–637. [CrossRef]
80. Xie, B.; Yang, F.; Chen, H.; Zhang, H.; Ma, H.; Li, T.; Chen, Z.; Li, J.; Li, X.; Du, J. Electrospun Polycaprolactone/Silk Fibroin Nanofiber Scaffold with Aligned Fiber Orientation for Articular Chondrocyte Regeneration. *Front. Mater.* **2023**, *10*, 1292098. [CrossRef]
81. Yang, L.; Wang, X.; Xiong, M.; Liu, X.; Luo, S.; Luo, J.; Wang, Y. Electrospun Silk Fibroin/Fibrin Vascular Scaffold with Superior Mechanical Properties and Biocompatibility for Applications in Tissue Engineering. *Sci. Rep.* **2024**, *14*, 3942. [CrossRef]
82. Rezvova, M.A.; Ovcharenko, E.A.; Klyshnikov, K.Y.; Glushkova, T.V.; Kostyunin, A.E.; Shishkova, D.K.; Matveeva, V.G.; Velikanova, E.A.; Shabaev, A.R.; Kudryavtseva, Y.A. Electrospun Bioresorbable Polymer Membranes for Coronary Artery Stents. *Front. Bioeng. Biotechnol.* **2024**, *12*, 1440181. [CrossRef]
83. Kyriakou, S.; Acosta, S.; El Maachi, I.; Rütten, S.; Jockenhoevel, S. A Dexamethasone-Loaded Polymeric Electrospun Construct as a Tubular Cardiovascular Implant. *Polymers* **2023**, *15*, 4332. [CrossRef]
84. Dolatyar, B.; Zeynali, B.; Shabani, I.; Tafreshi, A.P.; Karimi-Soflou, R. Enhanced Axonal Regeneration and Functional Recovery of the Injured Sciatic Nerve in a Rat Model by Lithium-Loaded Electrospun Nanofibrous Scaffolds. *Biodes Manuf.* **2024**, *7*, 701–720. [CrossRef]
85. Ikegami, Y.; Shafiq, M.; Aishima, S.; Ijima, H. Heparin/Growth Factors-Immobilized Aligned Electrospun Nanofibers Promote Nerve Regeneration in Polycaprolactone/Gelatin-Based Nerve Guidance Conduits. *Adv. Fiber Mater.* **2023**, *5*, 554–573. [CrossRef]
86. Shahrubudin, N.; Lee, T.C.; Ramlan, R. An Overview on 3D Printing Technology: Technological, Materials, and Applications. *Procedia Manuf.* **2019**, *35*, 1286–1296. [CrossRef]
87. Gokhare, V.G.; Raut, D.N.; Shinde, D.K. A Review Paper on 3D-Printing Aspects and Various Processes Used in the 3D-Printing. *Int. J. Eng. Res. Technol.* **2017**, *6*, 953–958.
88. Jandyal, A.; Chaturvedi, I.; Wazir, I.; Raina, A.; Ul Haq, M.I. 3D Printing—A Review of Processes, Materials and Applications in Industry 4.0. *Sustain. Oper. Comput.* **2022**, *3*, 33–42. [CrossRef]
89. Sahmani, S.; Khandan, A.; Esmaeili, S.; Saber-Samandari, S.; Ghadiri Nejad, M.; Aghdam, M.M. Calcium Phosphate-PLA Scaffolds Fabricated by Fused Deposition Modeling Technique for Bone Tissue Applications: Fabrication, Characterization and Simulation. *Ceram. Int.* **2020**, *46*, 2447–2456. [CrossRef]

90. Alizadeh-Osgouei, M.; Li, Y.; Vahid, A.; Ataee, A.; Wen, C. High Strength Porous PLA Gyroid Scaffolds Manufactured via Fused Deposition Modeling for Tissue-Engineering Applications. *Smart Mater. Med.* **2021**, *2*, 15–25. [CrossRef]
91. Xu, X.; Goyanes, A.; Trenfield, S.J.; Diaz-Gomez, L.; Alvarez-Lorenzo, C.; Gaisford, S.; Basit, A.W. Stereolithography (SLA) 3D Printing of a Bladder Device for Intravesical Drug Delivery. *Mater. Sci. Eng. C* **2021**, *120*, 111773. [CrossRef]
92. Guillaume, O.; Geven, M.A.; Sprecher, C.M.; Stadelmann, V.A.; Grijpma, D.W.; Tang, T.T.; Qin, L.; Lai, Y.; Alini, M.; de Bruijn, J.D.; et al. Surface-Enrichment with Hydroxyapatite Nanoparticles in Stereolithography-Fabricated Composite Polymer Scaffolds Promotes Bone Repair. *Acta Biomater.* **2017**, *54*, 386–398. [CrossRef]
93. Zhang, J.; Liu, J.; Wang, C.; Chen, F.; Wang, X.; Lin, K. A Comparative Study of the Osteogenic Performance between the Hierarchical Micro/Submicro-Textured 3D-Printed Ti6Al4V Surface and the SLA Surface. *Bioact. Mater.* **2020**, *5*, 9–16. [CrossRef]
94. Wiria, F.E.; Leong, K.F.; Chua, C.K.; Liu, Y. Poly-ε-Caprolactone/Hydroxyapatite for Tissue Engineering Scaffold Fabrication via Selective Laser Sintering. *Acta Biomater.* **2007**, *3*, 1–12. [CrossRef]
95. Yeong, W.Y.; Sudarmadji, N.; Yu, H.Y.; Chua, C.K.; Leong, K.F.; Venkatraman, S.S.; Boey, Y.C.F.; Tan, L.P. Porous Polycaprolactone Scaffold for Cardiac Tissue Engineering Fabricated by Selective Laser Sintering. *Acta Biomater.* **2010**, *6*, 2028–2034. [CrossRef] [PubMed]
96. Shuai, C.; Mao, Z.; Lu, H.; Nie, Y.; Hu, H.; Peng, S. Fabrication of Porous Polyvinyl Alcohol Scaffold for Bone Tissue Engineering via Selective Laser Sintering. *Biofabrication* **2013**, *5*, 015014. [CrossRef]
97. Liu, Z.; Liang, H.; Shi, T.; Xie, D.; Chen, R.; Han, X.; Shen, L.; Wang, C.; Tian, Z. Additive Manufacturing of Hydroxyapatite Bone Scaffolds via Digital Light Processing and in Vitro Compatibility. *Ceram. Int.* **2019**, *45*, 11079–11086. [CrossRef]
98. Cao, Y.; Shi, T.; Jiao, C.; Liang, H.; Chen, R.; Tian, Z.; Zou, A.; Yang, Y.; Wei, Z.; Wang, C.; et al. Fabrication and Properties of Zirconia/Hydroxyapatite Composite Scaffold Based on Digital Light Processing. *Ceram. Int.* **2020**, *46*, 2300–2308. [CrossRef]
99. Wang, J.; Tang, Y.; Cao, Q.; Wu, Y.; Wang, Y.; Yuan, B.; Li, X.; Zhou, Y.; Chen, X.; Zhu, X.; et al. Fabrication and Biological Evaluation of 3D-Printed Calcium Phosphate Ceramic Scaffolds with Distinct Macroporous Geometries through Digital Light Processing Technology. *Regen. Biomater.* **2022**, *9*, rbac005. [CrossRef]
100. Ataee, A.; Li, Y.; Brandt, M.; Wen, C. Ultrahigh-Strength Titanium Gyroid Scaffolds Manufactured by Selective Laser Melting (SLM) for Bone Implant Applications. *Acta Mater.* **2018**, *158*, 354–368. [CrossRef]
101. Kelly, C.N.; Francovich, J.; Julmi, S.; Safranski, D.; Guldberg, R.E.; Maier, H.J.; Gall, K. Fatigue Behavior of As-Built Selective Laser Melted Titanium Scaffolds with Sheet-Based Gyroid Microarchitecture for Bone Tissue Engineering. *Acta Biomater.* **2019**, *94*, 610–626. [CrossRef]
102. Attaeyan, A.; Shahgholi, M.; Khandan, A. Fabrication and Characterization of Novel 3D Porous Titanium-6Al-4V Scaffold for Orthopedic Application Using Selective Laser Melting Technique. *Iran. J. Chem. Chem. Eng. (IJCCE) Res. Artic.* **2024**, *43*, 66–82.
103. Kumar, S.; Singh, I.; Kumar, D.; Yahya, M.Y.; Rahimian Koloor, S.S. Mechanical and Morphological Characterizations of Laminated Object Manufactured 3D Printed Biodegradable Poly(Lactic)Acid with Various Physical Configurations. *J. Mar. Sci. Eng.* **2022**, *10*, 1954. [CrossRef]
104. Xu, C.; Yang, K.; Xu, Y.; Meng, X.; Zhou, Y.; Xu, Y.; Li, X.; Qiao, W.; Shi, J.; Zhang, D.; et al. Melt-Electrowriting-Enabled Anisotropic Scaffolds Loaded with Valve Interstitial Cells for Heart Valve Tissue Engineering. *J. Nanobiotechnol.* **2024**, *22*, 378. [CrossRef]
105. Xie, J.; Gao, Q.; del Prado, Z.N.; Venkateswaran, N.; Mousa, H.M.; Salero, E.; Ye, J.; De Juan-Pardo, E.M.; Sabater, A.L.; Perez, V.L. Establishment of a Bi-Layered Tissue Engineered Conjunctiva Using a 3D-Printed Melt Electrowritten Poly-(ε-Caprolactone) Scaffold. *Int. Ophthalmol.* **2023**, *43*, 215–232. [CrossRef] [PubMed]
106. Lai, X.; Huang, J.; Huang, S.; Wang, J.; Zheng, Y.; Luo, Y.; Tang, L.; Gao, B.; Tang, Y. Antibacterial and Osteogenic Dual-Functional Micronano Composite Scaffold Fabricated via Melt Electrowriting and Solution Electrospinning for Bone Tissue Engineering. *ACS Appl. Mater. Interfaces* **2024**, *16*, 37707–37721. [CrossRef] [PubMed]
107. Abdal-hay, A.; Kocak-Oztug, N.A.; Sheikh, F.A.; Han, P.; Anwar, S.; Fournier, B.P.J.; Ivanovski, S. Fabrication of 3D Bioactive Melt Electrowriting Composite Scaffold with High Osteogenic Potential. *Colloids Surf. B Biointerfaces* **2025**, *245*, 114270. [CrossRef]
108. Chennakesava, P.; Narayan, Y.S. Fused Deposition Modeling-Insights. In Proceedings of the International Conference on Advances in Design & Manufacturing (ICAD&M'14), Tiruchirappalli, Tamil Nadu, India, 5–7 December 2014.
109. Cano-Vicent, A.; Tambuwala, M.M.; Hassan, S.S.; Barh, D.; Aljabali, A.A.A.; Birkett, M.; Arjunan, A.; Serrano-Aroca, Á. Fused Deposition Modelling: Current Status, Methodology, Applications and Future Prospects. *Addit. Manuf.* **2021**, *47*, 102378. [CrossRef]
110. Kristiawan, R.B.; Imaduddin, F.; Ariawan, D.; Ubaidillah; Arifin, Z. A Review on the Fused Deposition Modeling (FDM) 3D Printing: Filament Processing, Materials, and Printing Parameters. *Open Eng.* **2021**, *11*, 639–649. [CrossRef]
111. Kafle, A.; Luis, E.; Silwal, R.; Pan, H.M.; Shrestha, P.L.; Bastola, A.K. 3d/4d Printing of Polymers: Fused Deposition Modelling (Fdm), Selective Laser Sintering (Sls), and Stereolithography (Sla). *Polymers* **2021**, *13*, 3101. [CrossRef]
112. Deshmane, S.; Kendre, P.; Mahajan, H.; Jain, S. Stereolithography 3D Printing Technology in Pharmaceuticals: A Review. *Drug Dev. Ind. Pharm.* **2021**, *47*, 1362–1372. [CrossRef]

113. Maines, E.M.; Porwal, M.K.; Ellison, C.J.; Reineke, T.M. Sustainable Advances in SLA/DLP 3D Printing Materials and Processes. *Green. Chem.* **2021**, *23*, 6863–6897. [CrossRef]
114. Huang, J.; Qin, Q.; Wang, J. A Review of Stereolithography: Processes and Systems. *Processes* **2020**, *8*, 1138. [CrossRef]
115. Gueche, Y.A.; Sanchez-Ballester, N.M.; Cailleaux, S.; Bataille, B.; Soulairol, I. Selective Laser Sintering (Sls), a New Chapter in the Production of Solid Oral Forms (Sofs) by 3d Printing. *Pharmaceutics* **2021**, *13*, 1212. [CrossRef]
116. Lekurwale, S.; Karanwad, T.; Banerjee, S. Selective Laser Sintering (SLS) of 3D Printlets Using a 3D Printer Comprised of IR/Red-Diode Laser. *Ann. 3D Print. Med.* **2022**, *6*, 100054. [CrossRef]
117. Charoo, N.A.; Barakh Ali, S.F.; Mohamed, E.M.; Kuttolamadom, M.A.; Ozkan, T.; Khan, M.A.; Rahman, Z. Selective Laser Sintering 3D Printing–an Overview of the Technology and Pharmaceutical Applications. *Drug Dev. Ind. Pharm.* **2020**, *46*, 869–877. [CrossRef]
118. Zhao, Z.; Tian, X.; Song, X. Engineering Materials with Light: Recent Progress in Digital Light Processing Based 3D Printing. *J. Mater. Chem. C Mater.* **2020**, *8*, 13896–13917. [CrossRef]
119. Chaudhary, R.; Fabbri, P.; Leoni, E.; Mazzanti, F.; Akbari, R.; Antonini, C. Additive Manufacturing by Digital Light Processing: A Review. *Progress. Addit. Manuf.* **2023**, *8*, 331–351. [CrossRef]
120. Cheng, J.; Yu, S.; Wang, R.; Ge, Q. Digital Light Processing Based Multimaterial 3D Printing: Challenges, Solutions and Perspectives. *Int. J. Extrem. Manuf.* **2024**, *6*, 042006. [CrossRef]
121. Gao, B.; Zhao, H.; Peng, L.; Sun, Z. A Review of Research Progress in Selective Laser Melting (SLM). *Micromachines* **2023**, *14*, 57. [CrossRef]
122. Yap, C.Y.; Chua, C.K.; Dong, Z.L.; Liu, Z.H.; Zhang, D.Q.; Loh, L.E.; Sing, S.L. Review of Selective Laser Melting: Materials and Applications. *Appl. Phys. Rev.* **2015**, *2*, 041101. [CrossRef]
123. Valino, A.D.; Dizon, J.R.C.; Espera, A.H.; Chen, Q.; Messman, J.; Advincula, R.C. Advances in 3D Printing of Thermoplastic Polymer Composites and Nanocomposites. *Prog. Polym. Sci.* **2019**, *98*, 101162. [CrossRef]
124. Park, J.; Tari, M.J.; Hahn, H.T. Characterization of the Laminated Object Manufacturing (LOM) Process. *Rapid Prototyp. J.* **2000**, *6*, 36–50. [CrossRef]
125. Dermeik, B.; Travitzky, N. Laminated Object Manufacturing of Ceramic-Based Materials. *Adv. Eng. Mater.* **2020**, *22*, 2000256. [CrossRef]
126. Asad, H.; Ihsanullah, K. A Review of Laminated Object Manufacturing (LOM) Aspects and Various Processes Used in It. *Int. J. Adv. Eng. Res. Sci.* **2023**, *10*, 46–54. [CrossRef]
127. Saiz, P.G.; Reizabal, A.; Vilas-Vilela, J.L.; Dalton, P.D.; Lanceros-Mendez, S. Materials and Strategies to Enhance Melt Electrowriting Potential. *Adv. Mater.* **2024**, *36*, 2312084. [CrossRef]
128. Dalton, P.D. Melt Electrowriting with Additive Manufacturing Principles. *Curr. Opin. Biomed. Eng.* **2017**, *2*, 49–57. [CrossRef]
129. Daghrery, A.; de Souza Araújo, I.J.; Castilho, M.; Malda, J.; Bottino, M.C. Unveiling the Potential of Melt Electrowriting in Regenerative Dental Medicine. *Acta Biomater.* **2023**, *156*, 88–109. [CrossRef] [PubMed]
130. O'Neill, K.L.; Dalton, P.D. A Decade of Melt Electrowriting. *Small Methods* **2023**, *7*, e2201589. [CrossRef] [PubMed]
131. Loewner, S.; Heene, S.; Baroth, T.; Heymann, H.; Cholewa, F.; Blume, H.; Blume, C. Recent Advances in Melt Electro Writing for Tissue Engineering for 3D Printing of Microporous Scaffolds for Tissue Engineering. *Front. Bioeng. Biotechnol.* **2022**, *10*, 896719. [CrossRef]
132. Ahmadi Bonakdar, M.; Rodrigue, D. Electrospinning: Processes, Structures, and Materials. *Macromol* **2024**, *4*, 58–103. [CrossRef]
133. Farsi, M.; Asefnejad, A.; Baharifar, H. A Hyaluronic Acid/PVA Electrospun Coating on 3D Printed PLA Scaffold for Orthopedic Application. *Prog. Biomater.* **2022**, *11*, 67–77. [CrossRef]
134. Kurowska, A.; Nikodem, A.; Jabłoński, A.; Janusz, J.; Szczygieł, P.; Ziąbka, M.; Menaszek, E.; Dziadek, M.; Zagrajczuk, B.; Kobielarz, M.; et al. Layered PCL Scaffolds Modified with Bioactive Additives Fabricated by Electrospinning and 3D-Printing for the Nasal Bone and Cartilage Defects. *Mater. Des.* **2023**, *233*, 112255. [CrossRef]
135. Romero-Araya, P.; Pino, V.; Nenen, A.; Cárdenas, V.; Pavicic, F.; Ehrenfeld, P.; Serandour, G.; Lisoni, J.G.; Moreno-Villoslada, I.; Flores, M.E. Combining Materials Obtained by 3D-Printing and Electrospinning from Commercial Polylactide Filament to Produce Biocompatible Composites. *Polymers* **2021**, *13*, 3806. [CrossRef]
136. Rezvani Ghomi, E.; Chellappan, V.; Neisiany, R.E.; Dubey, N.; Amuthavalli, K.; Verma, N.K.; Lakshminarayanan, R.; Ramakrishna, S. An Innovative Tunable Bimodal Porous PCL/Gelatin Dressing Fabricated by Electrospinning and 3D Printing for Efficient Wound Healing and Scalable Production. *Compos. Sci. Technol.* **2024**, *247*, 110402. [CrossRef]
137. Lou, L.; Rubfiaro, A.S.; Deng, V.; He, J.; Thomas, T.; Roy, M.; Dickerson, D.; Agarwal, A. Harnessing 3D Printing and Electrospinning for Multiscale Hybrid Patches Mimicking the Native Myocardium. *ACS Appl. Mater. Interfaces* **2024**, *16*, 37596–37612. [CrossRef]
138. Fazal, F.; Melchels, F.P.W.; McCormack, A.; Silva, A.F.; Handley, E.L.; Mazlan, N.A.; Callanan, A.; Koutsos, V.; Radacsi, N. Fabrication of a Compliant Vascular Graft Using Extrusion Printing and Electrospinning Technique. *Adv. Mater. Technol.* **2024**, *9*, 2400224. [CrossRef]

139. Rezaei, E.S.; Poursamar, S.A.; Naeimi, M.; Taheri, M.M.; Rafienia, M. An in Vitro and in Vivo Study of Electrospun Polyvinyl Alcohol/Chitosan/Sildenafil Citrate Mat on 3D-Printed Polycaprolactone Membrane as a Double Layer Wound Dressing. *Int. J. Biol. Macromol.* **2024**, *269*, 131859. [CrossRef] [PubMed]
140. Liu, J.; Zou, Q.; Wang, C.; Lin, M.; Li, Y.; Zhang, R.; Li, Y. Electrospinning and 3D Printed Hybrid Bi-Layer Scaffold for Guided Bone Regeneration. *Mater. Des.* **2021**, *210*, 110047. [CrossRef]
141. Song, Y.; Hu, Q.; Liu, S.; Wang, Y.; Zhang, H.; Chen, J.; Yao, G. Electrospinning/3D Printing Drug-Loaded Antibacterial Polycaprolactone Nanofiber/Sodium Alginate-Gelatin Hydrogel Bilayer Scaffold for Skin Wound Repair. *Int. J. Biol. Macromol.* **2024**, *275*, 129705. [CrossRef] [PubMed]
142. Cojocaru, E.; Ghitman, J.; Pircalabioru, G.G.; Zaharia, A.; Iovu, H.; Sarbu, A. Electrospun/3D-Printed Bicomponent Scaffold Co-Loaded with a Prodrug and a Drug with Antibacterial and Immunomodulatory Properties. *Polymers* **2023**, *15*, 2854. [CrossRef]
143. Pensa, N.W.; Curry, A.S.; Bonvallet, P.P.; Bellis, N.F.; Rettig, K.M.; Reddy, M.S.; Eberhardt, A.W.; Bellis, S.L. 3D Printed Mesh Reinforcements Enhance the Mechanical Properties of Electrospun Scaffolds. *Biomater. Res.* **2019**, *23*, 22. [CrossRef]
144. Atari, M.; Saroukhani, A.; Manshaei, M.; Bateni, P.; Zargar kharazi, A.; Vatankhah, E.; Haghjooy Javanmard, S. Preclinical in Vivo Assessment of a Cell-Free Multi-Layered Scaffold Prepared by 3D Printing and Electrospinning for Small-Diameter Blood Vessel Tissue Engineering in a Canine Model. *Biomater. Sci.* **2023**, *11*, 6871–6880. [CrossRef]
145. Chen, S.; Zheng, L.; Wang, M. 4D Bioprinted Tri-Layer Scaffolds with Biomimetic and Hierarchical Structure for Uterine Tissue Regeneration. In Proceedings of the Society For Biomaterials 2023 Annual Meeting & Exposition, San Diego, CA, USA, 19–22 April 2023.
146. Mirhaj, M.; Varshosaz, J.; Labbaf, S.; Emadi, R.; Marcus Seifalian, A.; Sharifianjazi, F. An Antibacterial Multi-Layered Scaffold Fabricated by 3D Printing and Electrospinning Methodologies for Skin Tissue Regeneration. *Int. J. Pharm.* **2023**, *645*, 123357. [CrossRef]
147. Belgheisi, G.; Haghbin Nazarpak, M.; Solati-Hashjin, M. Fabrication and Evaluation of Combined 3D Printed/Pamidronate-Layered Double Hydroxides Enriched Electrospun Scaffolds for Bone Tissue Engineering Applications. *Appl. Clay Sci.* **2022**, *225*, 106538. [CrossRef]
148. Zhu, Y.; Liu, X.; Zhang, K.; EL-Newehy, M.; Abdulhameed, M.M.; Mo, X.; Cao, L.; Wang, Y. Application of Electrospinning and 3D-Printing Based Bilayer Composite Scaffold in the Skull Base Reconstruction during Transnasal Surgery. *Colloids Surf. B Biointerfaces* **2025**, *245*, 114337. [CrossRef] [PubMed]
149. Yilmaz, H.; Bedir, T.; Gursoy, S.; Kaya, E.; Senel, I.; Tinaz, G.B.; Gunduz, O.; Ustundag, C.B. Development of Bilayer Tissue-Engineered Scaffolds: Combination of 3D Printing and Electrospinning Methodologies. *Biomed. Mater.* **2024**, *19*, 045029. [CrossRef]
150. Chen, Y.; Shafiq, M.; Liu, M.; Morsi, Y.; Mo, X. Advanced Fabrication for Electrospun Three-Dimensional Nanofiber Aerogels and Scaffolds. *Bioact. Mater.* **2020**, *5*, 963–979. [CrossRef]
151. He, W.; Li, C.; Zhao, S.; Li, Z.; Wu, J.; Li, J.; Zhou, H.; Yang, Y.; Xu, Y.; Xia, H. Integrating Coaxial Electrospinning and 3D Printing Technologies for the Development of Biphasic Porous Scaffolds Enabling Spatiotemporal Control in Tumor Ablation and Osteochondral Regeneration. *Bioact. Mater.* **2024**, *34*, 338–353. [CrossRef] [PubMed]
152. Chen, W.; Xu, Y.; Liu, Y.; Wang, Z.; Li, Y.; Jiang, G.; Mo, X.; Zhou, G. Three-Dimensional Printed Electrospun Fiber-Based Scaffold for Cartilage Regeneration. *Mater. Des.* **2019**, *179*, 107886. [CrossRef]
153. Cai, P.; Li, C.; Ding, Y.; Lu, H.; Yu, X.; Cui, J.; Yu, F.; Wang, H.; Wu, J.; EL-Newehy, M.; et al. Elastic 3D-Printed Nanofibers Composite Scaffold for Bone Tissue Engineering. *ACS Appl. Mater. Interfaces* **2023**, *15*, 54280–54293. [CrossRef]
154. Zarei, M.; Żwir, M.J.; Michalkiewicz, B.; Gorący, J.; El Fray, M. Template-Assisted Electrospinning and 3D Printing of Multilayered Hierarchical Vascular Grafts. *J. Biomed. Mater. Res. Part B Appl. Biomater.* **2025**, *113*, e35525. [CrossRef]
155. Song, J.Y.; Ryu, H.I.; Lee, J.M.; Bae, S.H.; Lee, J.W.; Yi, C.C.; Park, S.M. Conformal Fabrication of an Electrospun Nanofiber Mat on a 3D Ear Cartilage-Shaped Hydrogel Collector Based on Hydrogel-Assisted Electrospinning. *Nanoscale Res. Lett.* **2021**, *16*, 116. [CrossRef]
156. Holjevac Grgurić, T.; Mijović, B.; Zdraveva, E.; Govorčin Bajsić, E.; Slivac, I.; Ujčić, M.; Dekaris, I.; Tominac Trcin, M.; Vuković, A.; Kuzmić, S.; et al. Electrospinning of PCL/CEFUROXIM® Fibrous Scaffolds on 3D Printed Collectors. *J. Text. Inst.* **2020**, *111*, 1288–1299. [CrossRef]
157. Kasoju, N.; George, J.; Ye, H.; Cui, Z. Sacrificial Core-Based Electrospinning: A Facile and Versatile Approach to Fabricate Devices for Potential Cell and Tissue Encapsulation Applications. *Nanomaterials* **2018**, *8*, 863. [CrossRef] [PubMed]
158. Doan, M.A.; Tobos, C.I.; Creighton, R.L.; Guo, T.; Faber, K.A.; Han, Y.; Chiew, C.; Hull, I.T.; Malakooti, M.H.; Woodrow, K.A. High-Resolution 3D Deposition of Electrospun Fibers on Patterned Dielectric Elastomers. *Adv. Eng. Mater.* **2023**, *25*, 2300670. [CrossRef]
159. Brooks-Richards, T.L.; Paxton, N.C.; Allenby, M.C.; Woodruff, M.A. Dissolvable 3D Printed PVA Moulds for Melt Electrowriting Tubular Scaffolds with Patient-Specific Geometry. *Mater. Des.* **2022**, *215*, 110466. [CrossRef]

160. Carranza, T.; Uranga, J.; Irastorza, A.; Izeta, A.; Guerrero, P.; de la Caba, K. Combination of 3D Printing and Electrospinning to Develop Chitin/Gelatin/PVA Scaffolds. *Int. J. Bioprint.* **2023**, *9*, 701. [CrossRef]
161. Jiang, S.; Kang, Z.; Liu, F.; Fan, J. 2D and 3D Electrospinning of Nanofibrous Structures by Far-Field Jet Writing. *ACS Appl. Mater. Interfaces* **2023**, *15*, 23777–23782. [CrossRef]
162. Gonzalez-Pujana, A.; Carranza, T.; Santos-Vizcaino, E.; Igartua, M.; Guerrero, P.; Hernandez, R.M.; de la Caba, K. Hybrid 3D Printed and Electrospun Multi-Scale Hierarchical Polycaprolactone Scaffolds to Induce Bone Differentiation. *Pharmaceutics* **2022**, *14*, 2843. [CrossRef] [PubMed]
163. Wang, L.; Ma, S.; Zheng, S.; Li, D.; Hu, W. Near-Field Direct-Writing Electrostatic Spinning 3D Bionic Tendon-Bone Repair Scaffold and Preparation Method Thereof. China Patent CN115845136A, 28 March 2023. Available online: https://worldwide.espacenet.com/patent/search?q=pn=CN115845136A (accessed on 19 May 2025).
164. Liu, L.; Zhou, L. Composite 3D-Printing Forming System, Forming Method, and INTRAVascular Stent. China Patent CN106584836A, 26 April 2017. Available online: https://worldwide.espacenet.com/patent/search?q=pn=CN106584836A (accessed on 19 May 2025).
165. Cárdenas, A.W.A.; Lara, B.A.L.; Silva, C.I.Z. Method of Manufacturing a Medical Device Using 3D Printing and Electrospinning. WO2023170557A1, 14 September 2023. Available online: https://worldwide.espacenet.com/patent/search?q=pn=WO2023170557A1 (accessed on 19 May 2025).
166. Noh, I.S.; Roh, G.S.; Tran, H.N.; Janarthanan, G. A Biodegradable Meniscus Scaffold and Its Manufacturing Method. Korea Patent KR20220040773A, 31 March 2022. Available online: https://worldwide.espacenet.com/patent/search?q=pn=KR20220040773A (accessed on 19 May 2025).
167. Wang, T.; Zhu, Q.; Quan, D.; Liu, X.; Wu, Z.; Yan, L. Multi-Channel Peripheral Nerve Conduit and Preparation Method Thereof. China Patent CN109172036A, 11 January 2019. Available online: https://worldwide.espacenet.com/patent/search/family/064948466/publication/CN109172036A?q=pn=CN109172036A (accessed on 19 May 2025).
168. Qiao, Z.; Sun, B.; Chen, W.; Dai, K.; Wang, Y. Method for Preparing Tendon Scaffold by Using Three-Dimensional Printing and Electrostatic Spinning Technologies. China Patent CN108404213A, 17 August 2018. Available online: https://worldwide.espacenet.com/patent/search?q=pn=CN108404213A (accessed on 19 May 2025).
169. Sun, D.; Wu, H.; Xu, F.; Jin, H.; Xue, M.; Zhang, Z.; Chen, S.; He, G. Method for Promoting Myocardial Tissue Morphological Induction via Bioprinting with 3D Nanofiber Constraints and Its Application. China Patent CN118048298A, 5 February 2024. Available online: https://worldwide.espacenet.com/patent/search?q=pn=CN118048298A (accessed on 19 May 2025).
170. Zhang, G.; Huang, H.; Lan, H.; Li, W.; Song, D.; Wang, Z.; Peng, Z.; Zhao, J. Method for Preparing Conductive Biological Scaffold Based on Self-Excited Electrostatic Field Driven Melt-Jet Three-Dimensional (3D) Printing. China Patent CN112157906A, 1 January 2021. Available online: https://worldwide.espacenet.com/patent/search?q=pn=CN112157906A (accessed on 19 May 2025).
171. Breuer, C.; Best, C.; Strouse, R.; Hibino, N.; Ung-Lee, Y. Systems and Methods for Optimized Patient Specific Tissue Engineering Vascular Grafts. U.S. Patent US11541149B2, 3 January 2023. Available online: https://worldwide.espacenet.com/patent/search?q=pn=US11541149B2 (accessed on 19 May 2025).
172. Hu, Q.; Li, D.; Liu, L.; Jiang, C.; Liu, Y.; Li, S.; Liu, Y. Micro-Nano Composite Dual-Layer Skin Framework and Manufacturing Method Thereof. China Patent CN106110401A, 16 November 2016. Available online: https://worldwide.espacenet.com/patent/search?q=pn=CN106110401A (accessed on 19 May 2025).
173. Feng, J.; Zhao, J. Preparation Method of Multilayer Composite Nano-Micron Fiber Topological Morphology Scaffold Imitating ECM Structure. China Patent CN112121232A, 25 December 2020. Available online: https://worldwide.espacenet.com/patent/search?q=pn=CN112121232A (accessed on 19 May 2025).
174. Yeo, M.G.; Kim, M.S.; Lee, C.S.; Park, M.J.; Kim, S.M.; Jung, B.S.; Lee, J.W.; Son, K.H. Artificial Blood Vessel and the Manufacturing Method Thereof. Korea Patent KR102467263B1, 16 November 2022. Available online: https://worldwide.espacenet.com/patent/search?q=pn=KR102467263B1 (accessed on 19 May 2025).
175. Zhang, T.; Li, Y.; Bai, H.; Liu, H.; Wang, L.; Zhang, Y.; Wang, Y.; Zhang, H.; Feng, L.; Sun, L. Preparation Method of Bionic Blood Vessel Graft Based on Electrostatic Spinning and 3D Printing. China Patent CN109701079A, 30 April 2019. Available online: https://worldwide.espacenet.com/patent/search?q=pn=CN109701079A (accessed on 19 May 2025).
176. Liu, J.; Pang, Q.; Jiang, L.; Lin, J. Bionic Bone Tissue Engineering Scaffold Material and Preparation Method Thereof. China Patent CN115054728A, 16 September 2022. Available online: https://worldwide.espacenet.com/patent/search?q=pn=CN115054728A (accessed on 19 May 2025).
177. Korean Intellectual Property Office. Bio Tubular Scaffold for Fabricating Artificial Vascular and the Fabricating Method thereof. Korea Patent KR101751986B1, 30 June 2017. Available online: https://worldwide.espacenet.com/patent/search?q=pn=KR101751986B1 (accessed on 19 May 2025).

178. Jung, E.; Kim, I.; Cho, H. Artificial Esophagus Scaffold and Manufacturing Method Thereof. Korea Patent KR102347096B1, 5 January 2022. Available online: https://worldwide.espacenet.com/patent/search?q=pn=KR102347096B1 (accessed on 19 May 2025).
179. Liu, Y.; Zhang, F.; Chen, W.; Yan, F.; Zheng, L.; Yu, Y.; Hu, Q. Regeneration Bone Scaffold Forming System and Method Based on Comprehensive 3D Printing Formation. China Patent CN103341989A, 9 October 2013. Available online: https://worldwide.espacenet.com/patent/search?q=pn=CN103341989A (accessed on 19 May 2025).
180. Zhang, H.; Deng, K.; Yuan, Y. 3D Printing and Electrospinning Composite Scaffold for Cartilage Tissue Engineering and Preparation Method Thereof. China Patent CN106827496A, 13 June 2017. Available online: https://worldwide.espacenet.com/patent/search?q=pn=CN106827496A (accessed on 19 May 2025).
181. Matai, I.; Kaur, G.; Seyedsalehi, A.; McClinton, A.; Laurencin, C.T. Progress in 3D Bioprinting Technology for Tissue/Organ Regenerative Engineering. *Biomaterials* **2020**, *226*, 119536. [CrossRef]
182. Augustine, R.; Kalva, S.N.; Ahmad, R.; Zahid, A.A.; Hasan, S.; Nayeem, A.; McClements, L.; Hasan, A. 3D Bioprinted Cancer Models: Revolutionizing Personalized Cancer Therapy. *Transl. Oncol.* **2021**, *14*, 101015. [CrossRef]
183. De Mori, A.; Fernández, M.P.; Blunn, G.; Tozzi, G.; Roldo, M. 3D Printing and Electrospinning of Composite Hydrogels for Cartilage and Bone Tissue Engineering. *Polymers* **2018**, *10*, 285. [CrossRef]
184. De Pieri, A.; Byerley, A.M.; Musumeci, C.R.; Salemizadehparizi, F.; Vanderhorst, M.A.; Wuertz-Kozak, K. Electrospinning and 3D Bioprinting for Intervertebral Disc Tissue Engineering. *JOR Spine* **2020**, *3*, 901–915. [CrossRef]
185. Urciuolo, A.; Poli, I.; Brandolino, L.; Raffa, P.; Scattolini, V.; Laterza, C.; Giobbe, G.G.; Zambaiti, E.; Selmin, G.; Magnussen, M.; et al. Intravital Three-Dimensional Bioprinting. *Nat. Biomed. Eng.* **2020**, *4*, 901–915. [CrossRef] [PubMed]
186. Neuhäusler, A.; Rogg, K.; Schröder, S.; Spiehl, D.; Zora, H.; Arefaine, E.; Schettler, J.; Hartmann, H.; Blaeser, A. Electrospun Microfibers to Enhance Nutrient Supply in Bioinks and 3D-Bioprinted Tissue Precursors. *Biofabrication* **2024**, *17*, 015038. [CrossRef] [PubMed]

**Disclaimer/Publisher's Note:** The statements, opinions and data contained in all publications are solely those of the individual author(s) and contributor(s) and not of MDPI and/or the editor(s). MDPI and/or the editor(s) disclaim responsibility for any injury to people or property resulting from any ideas, methods, instructions or products referred to in the content.